A mathematical model of metabolic insulin signaling pathways

Ahmad R. Sedaghat, Arthur Sherman and Michael J. Quon

A mathematical model of metabolic insulin signaling pathways

AHMAD R. SEDAGHAT,[1] ARTHUR SHERMAN,[2] AND MICHAEL J. QUON[1]
[1]*Cardiology Branch, National Heart, Lung, and Blood Institute, and* [2]*Mathematical Research Branch, National Institute of Diabetes and Digestive and Kidney Diseases, National Institutes of Health, Bethesda, Maryland 20892*

Sedaghat, Ahmad R., Arthur Sherman, and Michael J. Quon. A mathematical model of metabolic insulin signaling pathways. *Am J Physiol Endocrinol Metab* 283: E1084–E1101, 2002. First published July 2, 2002; 10.1152/ajpendo.00571.2001.—We develop a mathematical model that explicitly represents many of the known signaling components mediating translocation of the insulin-responsive glucose transporter GLUT4 to gain insight into the complexities of metabolic insulin signaling pathways. A novel mechanistic model of postreceptor events including phosphorylation of insulin receptor substrate-1, activation of phosphatidylinositol 3-kinase, and subsequent activation of downstream kinases Akt and protein kinase C-ζ is coupled with previously validated subsystem models of insulin receptor binding, receptor recycling, and GLUT4 translocation. A system of differential equations is defined by the structure of the model. Rate constants and model parameters are constrained by published experimental data. Model simulations of insulin dose-response experiments agree with published experimental data and also generate expected qualitative behaviors such as sequential signal amplification and increased sensitivity of downstream components. We examined the consequences of incorporating feedback pathways as well as representing pathological conditions, such as increased levels of protein tyrosine phosphatases, to illustrate the utility of our model for exploring molecular mechanisms. We conclude that mathematical modeling of signal transduction pathways is a useful approach for gaining insight into the complexities of metabolic insulin signaling.

signal transduction; metabolism; insulin resistance; GLUT4

INSULIN IS AN ESSENTIAL peptide hormone discovered in 1921 that regulates metabolism (26). Interestingly, the ability of insulin to promote glucose uptake into tissues was not demonstrated until 1949 (27). In 1971, specific cell surface insulin receptors were identified (12). The discovery that insulin-stimulated glucose transport involves translocation of glucose transporters (e.g., GLUT4) from an intracellular compartment to the cell surface was made in 1980 (8, 53). Since genes encoding the human insulin receptor and GLUT4 were cloned in 1985 (10, 54) and 1989 (5, 13), respectively, steady progress has been made in identifying components of insulin signal transduction pathways leading from the insulin receptor to translocation of GLUT4 (see Ref. 32 for review).

On binding insulin, the insulin receptor undergoes receptor autophosphorylation and enhanced tyrosine kinase activity. Subsequently, intracellular substrates (e.g., insulin receptor substrate-1, IRS-1) are phosphorylated on tyrosine residues that serve as docking sites for downstream SH2 domain containing proteins, including the p85 regulatory subunit of phosphatidylinositide 3-kinase (PI 3-kinase). The p85 binding to phosphorylated IRS-1 results in activation of the p110 catalytic subunit of PI 3-kinase that catalyzes production of phosphoinositol lipids including phosphatidylinositol 3,4,5-trisphosphates [PI(3,4,5)P_3] that activate the Ser/Thr kinase 3-phosphoinositide-dependent protein kinase (PDK)-1. PDK-1 phosphorylates and activates other downstream kinases, including Akt and protein kinase C (PKC)-ζ, that mediate translocation of GLUT4. PTP1B is a protein tyrosine phosphatase (PTPase) that negatively regulates insulin signaling pathways by dephosphorylating the insulin receptor and IRS-1. Interestingly, IRS-1 and PTP1B upstream from Akt and PKC-ζ have recently been identified as substrates for these downstream kinases, suggesting that feedback mechanisms exist (9, 33, 38, 39). Elements downstream from Akt and PKC-ζ linking insulin signaling pathways with trafficking machinery for GLUT4 are unknown (34). Thus a complete understanding of mechanisms regulating the metabolic actions of insulin has remained elusive.

One reason it has been difficult to comprehend metabolic insulin signaling pathways is that determinants of signal specificity are poorly understood. Many signaling molecules are shared in common among pathways initiated by distinct receptors. Moreover, cross talk and feedback between a multitude of receptor-mediated pathways generate signaling networks rather than linear pathways. Without a theoretical framework, it is difficult to understand how complexities evident from experimental data determine cell behavior. Now that the human genome has been sequenced, it may be

---

possible to generate a vast experimental database for understanding cellular signaling. Alfred Gilman has founded The Alliance for Cellular Signaling (**http://www.cellularsignaling.org/**) with the goal of integrating relevant experimental data (temporal and spatial relationships of signaling inputs and outputs in a cell) into interacting theoretical models. This comprehensive approach may enable a full understanding of the complexities of cell signaling. In this spirit, we now develop a mathematical model of metabolic insulin signaling pathways that explicitly represents many known insulin signaling components. Our goal is to define a comprehensive model that not only accurately represents known experimental data but will also serve as a useful tool to generate and test hypotheses. This modeling approach may lead to novel insights regarding the molecular mechanisms underlying insulin signal transduction pathways that regulate metabolic actions of insulin.

MODEL DEVELOPMENT

We use our previously validated models of insulin receptor binding kinetics (57), receptor recycling (36), and GLUT4 translocation (35, 37) as subsystems in conjunction with a novel mechanistic representation of postreceptor signaling

pathways to generate a complete model with 21 state variables. This complete model is then extended to incorporate feedback pathways, and consequences of feedback are explored. Differential equations derived from the structure of the complete model were solved by use of a fourth order Runge-Kutta numerical integration routine (42), using the WinPP version of XPPAUT (available at **http://www.math.pitt.edu/~bard/xpp/xpp.html**; see APPENDIX A for complete list of equations, initial conditions, and model parameters; see **http://mrb.niddk.nih.gov/sherman** for WinPP source files used to run simulations). A sufficiently small step size (0.001 min) was used to ensure accurate numerical integrations for all state variables. First order kinetics were assumed except where noted.

Complete Model without Feedback

Insulin receptor binding subsystem. Our model of insulin receptor binding kinetics (57) (Fig. 1*A*) was extended here to include additional steps representing insulin receptor autophosphorylation and dephosphorylation (Fig. 1*B*). On binding the first molecule of insulin, the receptor is rapidly phosphorylated (1), resulting in receptors that may either bind another molecule of insulin or dissociate from the first molecule of insulin. Binding of a second molecule of insulin does not affect the phosphorylation state of the receptor, whereas receptor dephosphorylation occurs when insulin diffuses off of the receptor, leaving a free receptor. In addition,
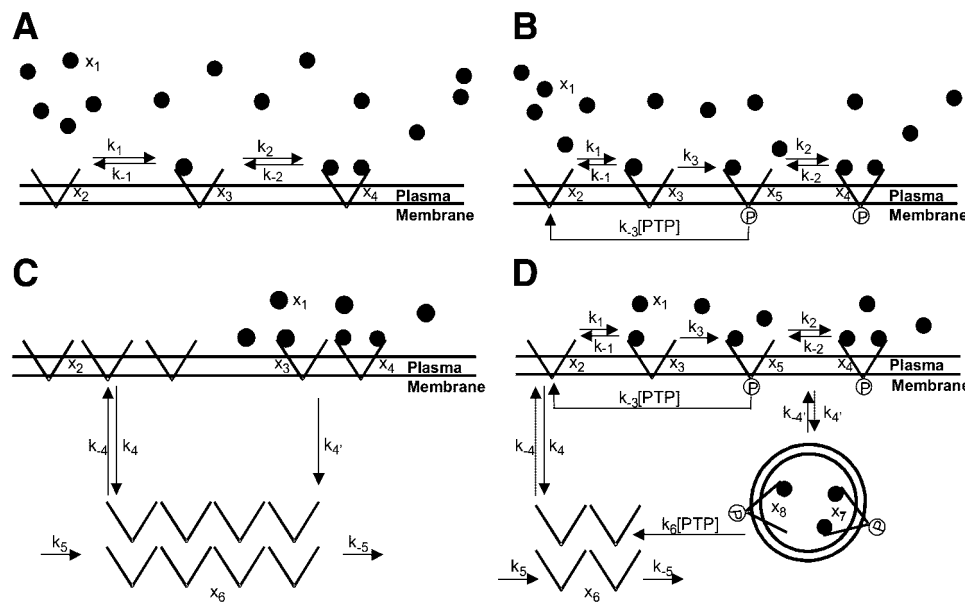
Fig. 1. Schematic of insulin receptor binding and life cycle subsystems. *A*: previously validated model of insulin binding kinetics (57). x_1, Free insulin concentration (system input); x_2, free receptor concentration; x_3, concentration of receptors with 1 molecule of insulin bound; x_4, concentration of receptors with 2 molecules of insulin bound; k_1 and k_{-1}, association and dissociation rate constants, respectively, for the first molecule of insulin to bind the receptor; k_2 and k_{-2}, association and dissociation rate constants, respectively, for the second molecule of insulin to bind the receptor. *B*: receptor binding subsystem extended to include receptor autophosphorylation and dephosphorylation. x_5, Concentration of once-bound phosphorylated receptors; x_4, redefined as concentration of twice-bound phosphorylated receptors; k_3, rate constant for receptor autophosphorylation; k_{-3}, rate constant for receptor dephosphorylation; [PTP], a multiplicative factor modulating k_{-3} that represents the relative activity of protein tyrosine phosphatases (PTPases) in the cell that dephosphorylate the insulin receptor. *C*: previously validated model of insulin receptor recycling (36). x_6, Concentrations of intracellular receptors; k_4, endocytosis rate constant for free receptors; k_{-4}, exocytosis rate constant; $k_{4'}$, endocytosis rate constant for bound receptors; k_5, zero order rate constant for receptor synthesis; k_{-5}, constant for receptor degradation. *D*: extension of insulin receptor binding and recycling subsystems that includes phosphorylated receptors. x_7 and x_8, concentration of twice-bound and once-bound intracellular phosphorylated receptors, respectively; $k_{-4'}$, exocytosis rate for twice-bound and once-bound intracellular phosphorylated receptors; k_6, dephosphorylation rate constant for intracellular receptors that is modulated by the multiplicative factor [PTP].

protein tyrosine phosphatases that dephosphorylate the insulin receptor and whose levels can vary under pathological conditions (15) are explicitly represented as a multiplicative factor ([PTP]) that modulates receptor dephosphorylation rate. The differential equations for this subsystem are

$$x_1 = \text{insulin input} \tag{1}$$

$$dx_2/dt = k_{-1}x_3 + k_{-3}[\text{PTP}]x_5 - k_1x_1x_2 \tag{2}$$

$$dx_3/dt = k_1x_1x_2 - k_{-1}x_3 - k_3x_3 \tag{3}$$

$$dx_4/dt = k_2x_1x_5 - k_{-2}x_4 \tag{4}$$

$$dx_5/dt = k_3x_3 + k_{-2}x_4 - k_2x_1x_5 - k_{-3}[\text{PTP}]x_5 \tag{5}$$

Definitions for state variables and rate constants are given in legend to Fig. 1, *A* and *B*. Note that we do not explicitly include an intermediate state of free receptors that are still phosphorylated because receptor occupancy and phosphorylation are tightly coupled, and we assume that there are virtually no receptors in the unbound phosphorylated state.

Insulin receptor recycling subsystem. Our previous model of insulin receptor life cycle explicitly represents synthesis, degradation, exocytosis, and both basal and ligand-induced endocytosis of receptors (36) (Fig. 1*C*). We now extend this subsystem so that ligand-induced endocytosis is only applied to phosphorylated cell surface receptors (Fig. 1*D*). Both once- and twice-bound phosphorylated receptors are treated identically with respect to internalization. An additional step representing dephosphorylation of internalized phosphorylated receptors and their incorporation into the intracellular pool is included. State variables representing free surface insulin receptors (x_2) and phosphorylated surface receptors (x_4 and x_5) are shared by both binding and recycling subsystems. Thus differential equations for these coupled subsystems (depicted in Fig. 1*D*) are

$$x_1 = \text{insulin input} \tag{6}$$

$$dx_2/dt = k_{-1}x_3 + k_{-3}[\text{PTP}]x_5 - k_1x_1x_2 + k_{-4}x_6 - k_4x_2 \tag{7}$$

$$dx_3/dt = k_1x_1x_2 - k_{-1}x_3 - k_3x_3 \tag{8}$$

$$dx_4/dt = k_2x_1x_5 - k_{-2}x_4 + k_{-4'}x_7 - k_{4'}x_4 \tag{9}$$

$$dx_5/dt = k_3x_3 + k_{-2}x_4 - k_2x_1x_5 - k_{-3}[\text{PTP}]x_5 \\ + k_{-4'}x_8 - k_{4'}x_5 \tag{10}$$

$$dx_6/dt = k_5 - k_{-5}x_6 + k_6[\text{PTP}](x_7 + x_8) + k_4x_2 - k_{-4}x_6 \tag{11}$$

$$dx_7/dt = k_{4'}x_4 - k_{-4'}x_7 - k_6[\text{PTP}]x_7 \tag{12}$$

$$dx_8/dt = k_{4'}x_5 - k_{-4'}x_8 - k_6[\text{PTP}]x_8 \tag{13}$$

Definitions for additional state variables and rate constants are given in legend to Fig. 1, *C* and *D*.

Postreceptor signaling subsystem. The postreceptor signaling subsystem developed here (Fig. 2) comprises elements in the metabolic insulin signaling pathway that are well established (32). It is assumed that this is a closed subsystem so that synthesis and degradation of signaling molecules are not explicitly represented. The concentration of phosphorylated surface insulin receptors is the input to this subsystem. Activated insulin receptors phosphorylate IRS-1, which then binds and activates PI 3-kinase. We modeled the dependence of IRS-1 phosphorylation on phosphorylated surface receptors as a linear function. That is, the rate constant for IRS-1 phosphorylation, k_7, is modulated by the fraction of phosphorylated surface receptors $(x_4 + x_5)/(\text{IR}_\text{p})$, where IR_p is the concentration of phosphorylated surface receptors achieved after maximal insulin stimulation. The association of phosphorylated IRS-1 with PI 3-kinase is assumed to occur with a
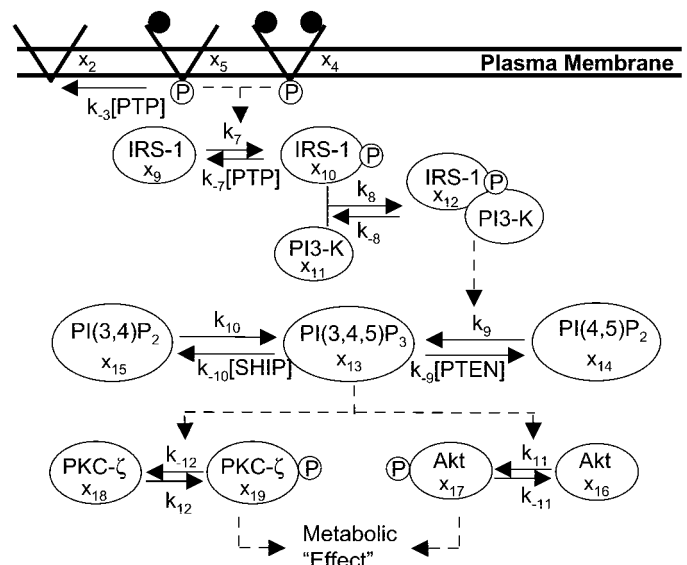

Fig. 2. Schematic of postreceptor signaling subsystem. x_9, Concentration of unphosphorylated insulin receptor substrate (IRS)-1; x_{10}, concentration of tyrosine-phosphorylated IRS-1; x_{11}, concentration of free phosphatidylinositol 3-kinase (PI 3-kinase; PI3-K); x_{12}, concentration of the phosphorylated IRS-1/activated PI 3-kinase complex; x_{13}, x_{14}, and x_{15}, percentages of various phosphoinositol lipids in the cell; x_{16} and x_{17}, percentages of unphosphorylated and phosphorylated Akt in the cell, respectively; x_{18} and x_{19}, percentages of unphosphorylated and phosphorylated protein kinase C (PKC)-ζ in the cell, respectively. The rate constants k_7 to k_{12} and k_{-7} to k_{-12} govern the conversion between state variables as indicated. [PTP] is a multiplicative factor modulating k_{-7} that represents the relative activity of PTPases in the cell that dephosphorylate IRS-1. [PTEN] and [SHIP] are multiplicative factors modulating k_{-9} and k_{-10}, respectively, that represent the relative activity of these lipid phosphatases in the cell. Arrows with solid lines indicate first-order reactions. Arrows with dashed lines indicate reactions where the value of a state variable influences the value of the rate constant.

stoichiometry of 1:1. Differential equations governing phosphorylation of IRS-1 and subsequent formation of phosphorylated IRS-1/activated PI 3-kinase complex are

$$dx_9/dt = k_{-7}[\text{PTP}]x_{10} - k_7x_9(x_4 + x_5)/(\text{IR}_\text{p}) \tag{14}$$

$$dx_{10}/dt = k_7x_9(x_4 + x_5)/(\text{IR}_\text{p}) \\ + k_{-8}x_{12} - (k_{-7}[\text{PTP}] + k_8x_{11})x_{10} \tag{15}$$

$$dx_{11}/dt = k_{-8}x_{12} - k_8x_{10}x_{11} \tag{16}$$

$$dx_{12}/dt = k_8x_{10}x_{11} - k_{-8}x_{12} \tag{17}$$

Activated PI 3-kinase converts the substrate phosphatidylinositol 4,5-bisphosphate [PI(4,5)P$_2$] to the product PI(3,4,5)P$_3$. This is modeled as a linear function so that k_9, the rate constant for generation of PI(3,4,5)P$_3$, is dependent on x_{12}, the amount of activated PI 3-kinase (see APPENDIX B for detailed derivation). 5′-Lipid phosphatases such as SHIP2 convert PI(3,4,5)P$_3$ to phosphatidylinositol 3,4-bisphosphate PI(3,4)P$_2$] (6), whereas 3′-lipid phosphatases such as PTEN convert PI(3,4,5)P$_3$ to PI(4,5)P$_2$ (45). The differential equations describing interconversion between these phosphatidylinositides are

$$dx_{13}/dt = k_9x_{14} + k_{10}x_{15} - (k_{-9}[\text{PTEN}] + k_{-10}[\text{SHIP}])x_{13} \tag{18}$$

$$dx_{14}/dt = k_{-9}[\text{PTEN}]x_{13} - k_9x_{14} \tag{19}$$

$$dx_{15}/dt = k_{-10}[\text{SHIP}]x_{13} - k_{10}x_{15} \tag{20}$$

As with [PTP], the lipid phosphatase factors [SHIP] and [PTEN] correspond to the relative phosphatase activity in the cell and are assigned a value of 1 under normal physiological conditions.

Activation of downstream Ser/Thr kinases Akt and PKC-ζ is dependent on levels of PI(3,4,5)P$_3$ (2, 49). In our model, this is governed by rate constants that interact with the level of PI(3,4,5)P$_3$ (see APPENDIX B for detailed derivation). The differential equations describing this are

$$dx_{16}/dt = k_{-11}x_{17} - k_{11}x_{16} \tag{21}$$

$$dx_{17}/dt = k_{11}x_{16} - k_{-11}x_{17} \tag{22}$$

$$dx_{18}/dt = k_{-12}x_{19} - k_{12}x_{18} \tag{23}$$

$$dx_{19}/dt = k_{12}x_{18} - k_{-12}x_{19} \tag{24}$$

The output of this subsystem is represented as a metabolic "Effect" due to Akt and PKC-ζ activity, with 80% of the metabolic insulin signaling effect attributed to PKC-ζ and 20% of the effect attributed to Akt (3, 7, 49)

$$\text{Effect} = (0.2x_{17} + 0.8x_{19})/(\text{AP}_{\text{equil}}) \tag{25}$$

where AP$_{\text{equil}}$ is the steady-state level of combined activity for Akt and PKC-ζ after maximal insulin stimulation (normalized to 100%). Definitions for additional state variables and rate constants in the postreceptor signaling subsystem are given in the legend to Fig. 2.

GLUT4 translocation subsystem. The final subsystem is our previous model of GLUT4 translocation (35, 37) (Fig. 3). Under basal conditions, GLUT4 recycles between an intracellular compartment and the cell surface. The differential equations for this subsystem are

$$dx_{20}/dt = k_{-13}x_{21} - (k_{13} + k_{13'})x_{20} + k_{14} - k_{-14}x_{20} \tag{26}$$

$$dx_{21}/dt = (k_{13} + k_{13'})x_{20} - k_{-13}x_{21} \tag{27}$$

Definitions for additional state variables and rate constants in the GLUT4 translocation subsystem are given in the legend to Fig. 3. On insulin stimulation, there may be a separate pool of intracellular GLUT4 recruited to the cell surface (17, 18, 40). To represent this aspect of GLUT4 trafficking, the insulin-stimulated exocytosis rate ($k_{13'}$) is

increased to its maximum value as a linear function of the metabolic effect produced by phosphorylated Akt and PKC-ζ. By assuming that the basal equilibrium distribution of 4% cell surface GLUT4 and 96% GLUT4 in the intracellular pool transitions on maximal insulin stimulation to a new steady state of 40% cell surface GLUT4 and 60% intracellular GLUT4, the equations governing changes in k_{13} and $k_{13'}$ are

$$k_{13} = (4/96)k_{-13} \tag{28}$$

$$k_{13'} = [(40/60) - (4/96)]k_{-13} \cdot (\text{Effect}) \tag{29}$$

Thus changes in $k_{13'}$ are linearly dependent on the output of the signaling subsystem (Effect).

For our complete model without feedback, the four subsystems described above were coupled by shared common elements (Fig. 4) (see APPENDIX B for derivation of initial conditions, rate constants, and parameters).

Complete Model with Feedback

Recent evidence suggests that Akt and PKC-ζ may participate in positive and negative feedback in metabolic insulin signaling pathways (9, 33, 38, 39). To investigate potential functional consequences of these feedback pathways, we incorporated both positive and negative feedback loops into our complete model (Fig. 5). Phosphorylation of PTP1B by Akt impairs the ability of PTP1B to dephosphorylate insulin receptors and IRS-1 by 25% (38). Because PTP1B itself negatively modulates insulin signaling, the downstream negative regulation of an upstream negative signaling element represents a positive feedback loop for insulin signaling. We implemented this positive feedback loop by assuming a linear effect of activated Akt (x_{17}) to inhibit PTP1B activity with a 25% decrease in [PTP] at maximal insulin stimulation. Thus [PTP] is multiplied by $1 - 0.25x_{17}/(100/11)$ (where 100/11 is the percentage of activated Akt after maximal insulin stimulation and for $x_{17} \leq 400/11$; otherwise, [PTP] = 0; see APPENDIX B for derivation).

We also incorporated a negative feedback loop in which serine phosphorylation of IRS-1 by PKC-ζ impairs formation of the phosphorylated IRS-1/activated PI 3-kinase complex (39). To represent this, we assumed that serine phosphory-
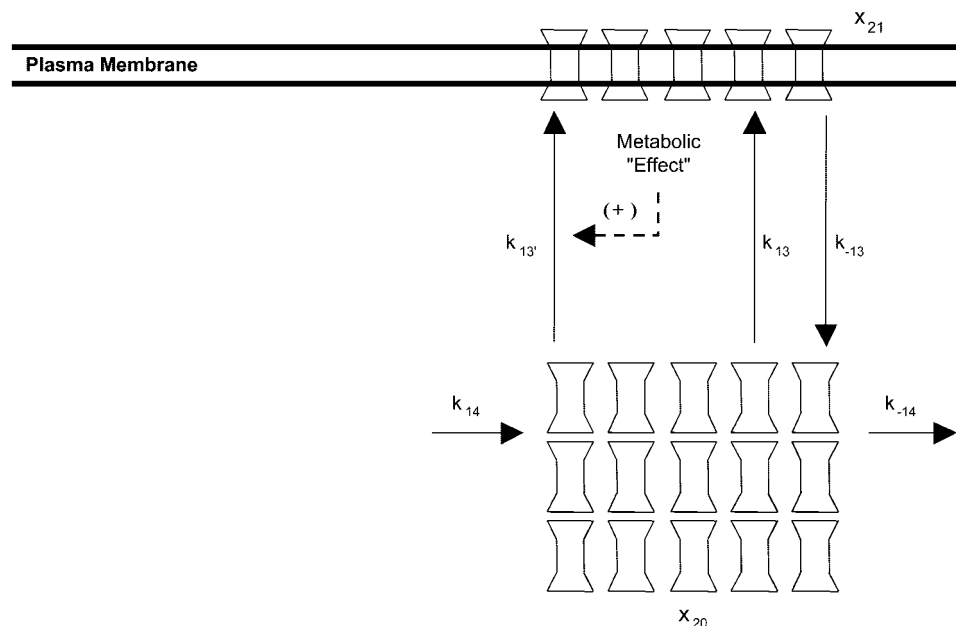
Fig. 3. Schematic of GLUT4 translocation subsystem (35, 37). x_{20}, Percentage of intracellular GLUT4; x_{21}, percentage of GLUT4 at the cell surface; k_{-13}, rate constant for GLUT4 internalization; k_{13}, rate constant for translocation of GLUT4 to the cell surface under basal conditions; $k_{13'}$, rate constant for translocation of GLUT4; k_{14} (zero order) and k_{-14}, rate constants for GLUT4 synthesis and degradation, respectively. The "metabolic Effect" from postreceptor signaling subsystem increases $k_{13'}$.

Fig. 4. Complete model of metabolic insulin signaling pathways obtained by coupling subsystem models for insulin receptor binding, receptor recycling, postreceptor signaling, and GLUT4 translocation.
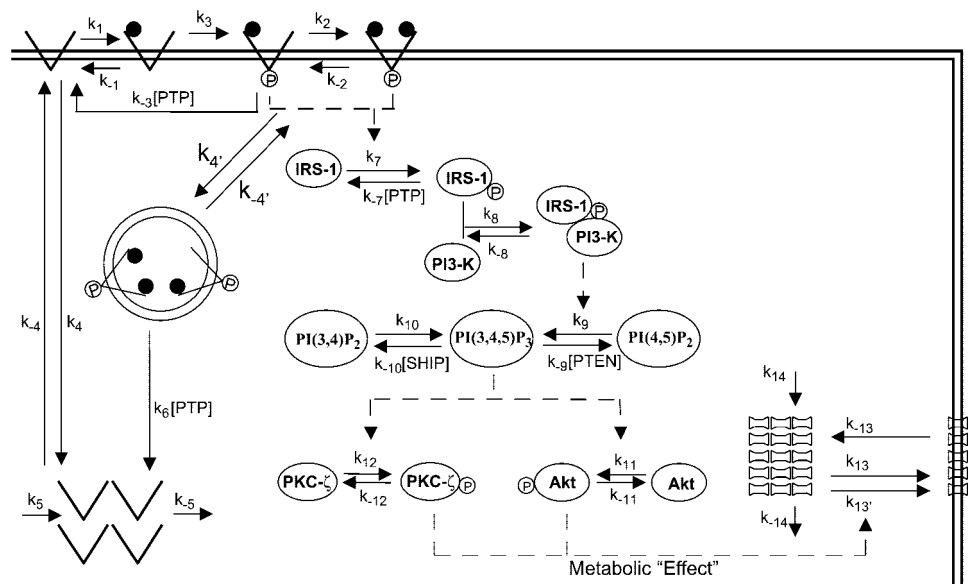
lation of IRS-1 by activated PKC-ζ creates an IRS-1 species unable to associate with and activate PI 3-kinase (represented by the state variable x_{10a}). The formation of x_{10a} tends to decrease the level of activated PI 3-kinase in response to insulin stimulation (when compared with a system without negative feedback). Additional differential equations describing interconversion between unphosphorylated IRS-1 (x_9) and serine-phosphorylated IRS-1 (x_{10a}) are

$$dx_9/dt = k_{-7}[\text{PTP}]x_{10} - k_7x_9(x_4 + x_5)/$$

$$(\text{IR}_p) + k_{-7'}x_{10a} - k_{7'}[\text{PKC}]x_9 \quad (30)$$

$$dx_{10a}/dt = k_{7'}[\text{PKC}]x_9 - k_{-7'}x_{10a} \quad (31)$$

where *Eq. 30* is an updated version of *Eq. 14*, $k_{7'}$ is the rate constant for serine phosphorylation of IRS-1 by PKC-ζ, and $k_{-7'}$ is the rate constant for serine dephosphorylation. We include a multiplicative factor, [PKC], that modulates $k_{7'}$ to model the ability of phosphorylated, activated PKC-ζ (x_{19}) to generate serine-phosphorylated IRS-1. [PKC] is defined as a

standard Hill equation that is commonly used to represent enzyme kinetics, where $[\text{PKC}] = V_{\max}x_{19}(t - \tau)^n/[K_d^n + x_{19}(t - \tau)^n]$, where $V_{\max}$ is maximal velocity and K_d is dissociation constant. This explicitly incorporates a time lag (τ) into the negative feedback loop. The parameters used in this equation are listed in APPENDIX A.

RESULTS

Model Simulations without Feedback

We began evaluation of our complete model without feedback by generating time courses for all state variables in response to a maximally stimulating step input of 10^{-7} M insulin that was turned off after 15 min (Figs. 6 and 7). Thirty seconds after the initial insulin stimulation, ~98% of the free insulin receptors became bound to insulin and underwent autophosphorylation (Fig. 6, *A–C*). Phosphorylated once-bound insulin re-

Fig. 5. Complete model of metabolic insulin signaling pathways with feedback. Identical to model shown in Fig. 4 except that new elements comprising positive and negative feedback pathways are indicated by dotted lines. PKC-ζ serine phosphorylates IRS-1 to create a negative feedback pathway, and Akt phosphorylates PTP1B to create a positive feedback pathway.

A

B

C

D
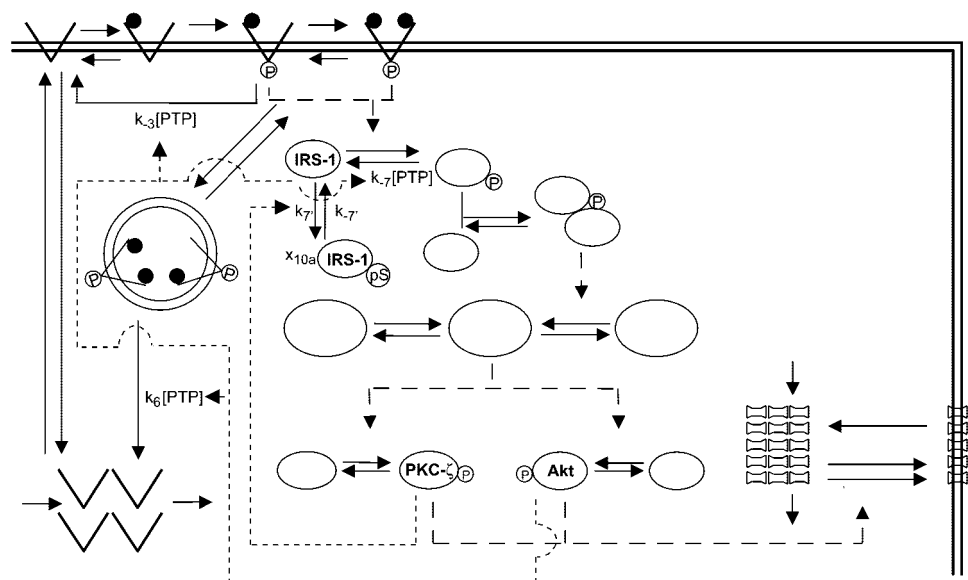
Fig. 6. Model simulations without feedback. Time courses for unbound receptors (*A*), once- and twice-bound phosphorylated surface receptors (*B*), total phosphorylated surface receptors (*C*), and unphosphorylated and tyrosine-phosphorylated IRS-1 (*D*) after a step input of 10^{-7} M insulin for 15 min.

A

B

C

D

Fig. 7. Model simulations without feedback. Time courses for activated PI 3-kinase (*A*), levels of phosphatidylinositol 3,4,5-trisphosphate [PI(3,4,5)P₃] and phosphatidylinositol 3,4-bisphosphate PI(3,4)P₂] (*B*), activated PKC-ζ (*C*), and cell surface GLUT4 (*D*) after a step input of 10^{-7} M insulin for 15 min.

ceptors at the cell surface made up ~75% of the surface receptor population, and phosphorylated twice-bound surface receptors comprised ~23% of the surface receptor population. When insulin was removed after 15 min of stimulation, the concentration of free insulin receptors returned to basal levels with a half-time of ~3.5 min. A short transient rise in the concentration of phosphorylated surface receptors bound to one molecule of insulin was observed as phosphorylated twice-bound surface receptors passed through the once-bound state to return to the unbound free state. As expected, the state variables x_6, x_7, and x_8, which represent intracellular insulin receptors, did not change very much with an acute insulin stimulation (data not shown). These results are in good agreement with both published experimental data and previous results from our subsystem models of receptor binding and recycling (36, 51, 57). In response to the rise in autophosphorylated surface insulin receptors, unphosphorylated IRS-1 was rapidly converted to tyrosine-phosphorylated IRS-1 (Fig. 6D). Consistent with published experimental data (29), maximal IRS-1 tyrosine phosphorylation was observed within 1 min of the initiation of insulin stimulation. On removal of insulin, IRS-1 underwent dephosphorylation back to basal conditions with a half-time of ~8 min. This was also consistent with published experimental data (24).

Maximal formation of the phosphorylated IRS-1/activated PI 3-kinase complex in response to 10^{-7} M insulin occurred within ~1.5 min (Fig. 7A). This is in good agreement with published data showing that PI3-kinase and tyrosine-phosphorylated IRS-1 molecules associate quickly after insulin stimulation (2, 14). The time course for disappearance of activated PI 3-kinase after the removal of insulin followed the time course for dephosphorylation of IRS-1. PI 3-kinase activated in response to insulin stimulation catalyzed the conversion of PI(4,5)P$_2$ to PI(3,4,5)P$_3$, which in turn drove the formation of PI(3,4)P$_2$ (Fig. 7B). The level of PI(3,4,5)P$_3$ increased from 0.31 to 3.1% of the total lipid population, and the level of PI(3,4)P$_2$ increased from 0.29 to 2.9% of the total lipid population as it equilibrated with PI(3,4,5)P$_3$. On removal of insulin, the phosphatidylinositides returned to basal levels (time to half-maximal levels was ~11 min). The levels of PI(3,4,5)P$_3$ controlled the formation of phosphorylated, activated PKC-ζ (Fig. 7C). Maximal PKC-ζ activation occurred within 3 min of insulin stimulation. After insulin was removed, the level of activated PKC-ζ declined back to basal levels (time to half-maximal levels was ~11 min). The time course for phosphorylated, activated Akt was identical to that for PKC-ζ (data not shown). Insulin-stimulated activation of PKC-ζ and Akt mediates increased exocytosis of GLUT4 so that 40% of total cellular GLUT4 was at the cell surface and 60% was intracellular after maximal insulin stimulation (Fig. 7D). Our simulations of insulin-stimulated GLUT4 recruitment occurred with a half-time of ~3 min, matching published experimental results (18, 20). When insulin was removed, surface and intracellular GLUT4 levels returned to their basal values (time to half-

maximal levels was ~16 min). Thus the overall response of our complete model without feedback to an acute insulin input is in good agreement with both a variety of published experimental data and previously validated subsystem models.

Model Simulations with Feedback

Having developed a plausible mechanistic model of metabolic insulin signaling pathways related to translocation of GLUT4, we next explored the effects of including positive and negative feedback loops to gain additional insight into the complexities of insulin signaling. Phosphorylation of PTP1B by Akt partially inhibits the ability of PTP1B to dephosphorylate the insulin receptor and IRS-1 (38). In addition, PKC-ζ phosphorylates serine residues on IRS-1 and inhibits the ability of IRS-1 to bind and activate PI 3-kinase (39). As described in MODEL DEVELOPMENT, we incorporated these positive and negative feedback interactions into our model. As for the model without feedback, we generated time courses for all state variables in response to a maximally stimulating step input of 10^{-7} M insulin for 15 min (Figs. 8 and 9). Time courses for the various insulin receptor states in response to insulin stimulation were qualitatively similar to results obtained from our model without feedback (cf. Fig. 6). However, after removal of insulin, the return of free surface receptors to basal levels and the disappearance of total phosphorylated surface receptors occurred a little more slowly than in the model without feedback. These results are consistent with the presence of a positive feedback loop at the level of the insulin receptor. With incorporation of negative feedback at the level of IRS-1, the time course for IRS-1 tyrosine phosphorylation in response to insulin stimulation is quite different from model simulations generated without feedback. In response to insulin, the level of tyrosine-phosphorylated IRS-1 transiently reached a peak of 0.84 pM within 1.5 min. This was followed by a rapid 60% decrease before a final equilibration at ~0.30 pM by 11 min (Fig. 8D). Thus the presence of negative feedback at the level of IRS-1 caused transient oscillatory behavior and a lower steady-state level for tyrosine-phosphorylated IRS-1. Levels of serine-phosphorylated IRS-1 first began to rise after 1.5 min of insulin stimulation. Similar to tyrosine-phosphorylated IRS-1, the concentration of serine-phosphorylated IRS-1 equilibrated at 0.76 pM after 5 min of insulin stimulation. Less than 10% of the total IRS-1 remained in the unactivated state after maximal insulin stimulation. Removal of insulin resulted in conversion of both serine- and tyrosine-phosphorylated IRS-1 back to unphosphorylated IRS-1 (time to return to half-maximal levels was ~17 min).

The transient oscillatory behavior observed for tyrosine-phosphorylated IRS-1 in response to insulin stimulation was also observed for activated PI 3-kinase (Fig. 9A). Activated PI 3-kinase transiently peaked at 5.6 fM within 1.8 min. This was followed by a rapid undershoot and then equilibration at ~1.9 fM by 10
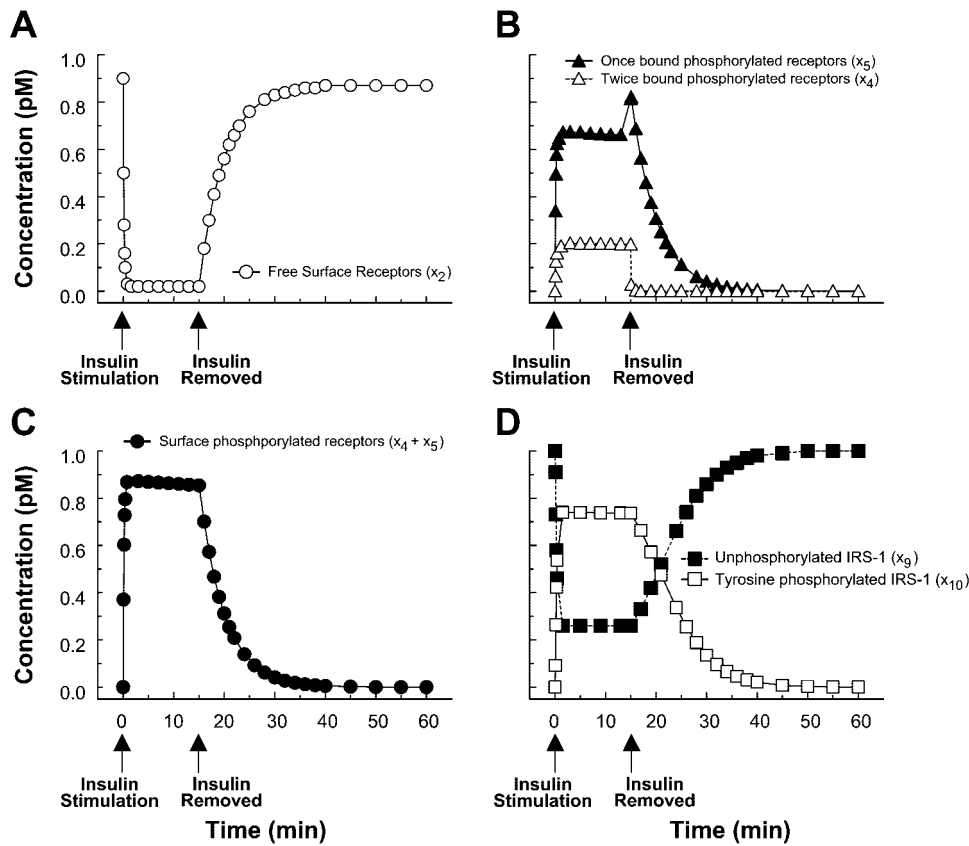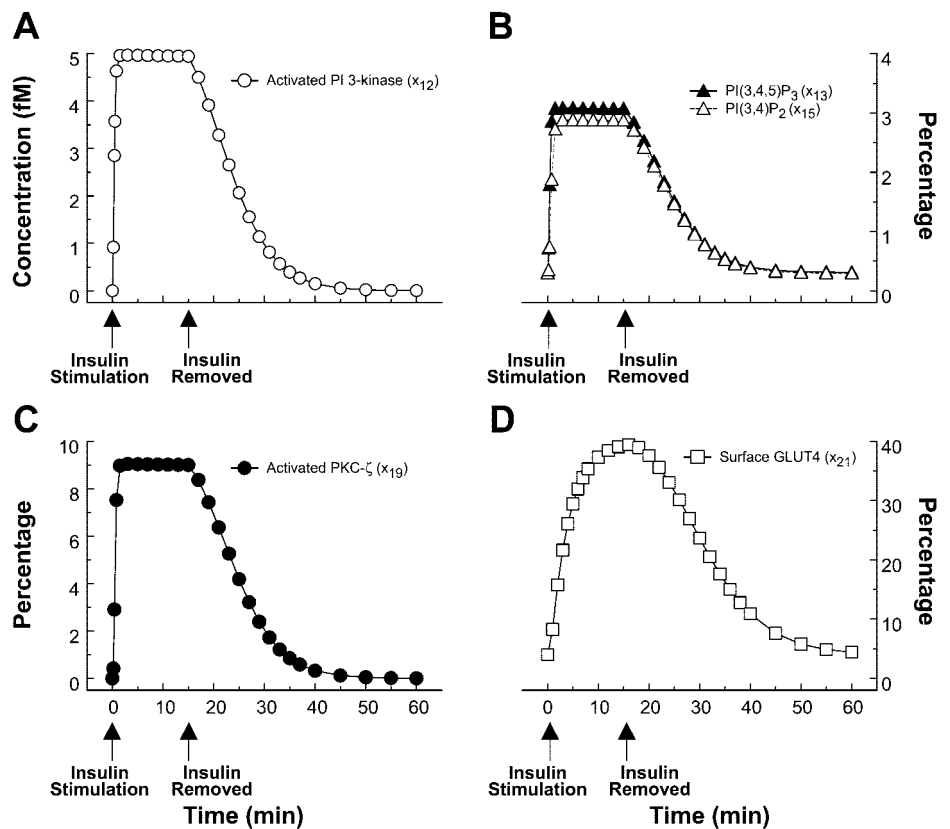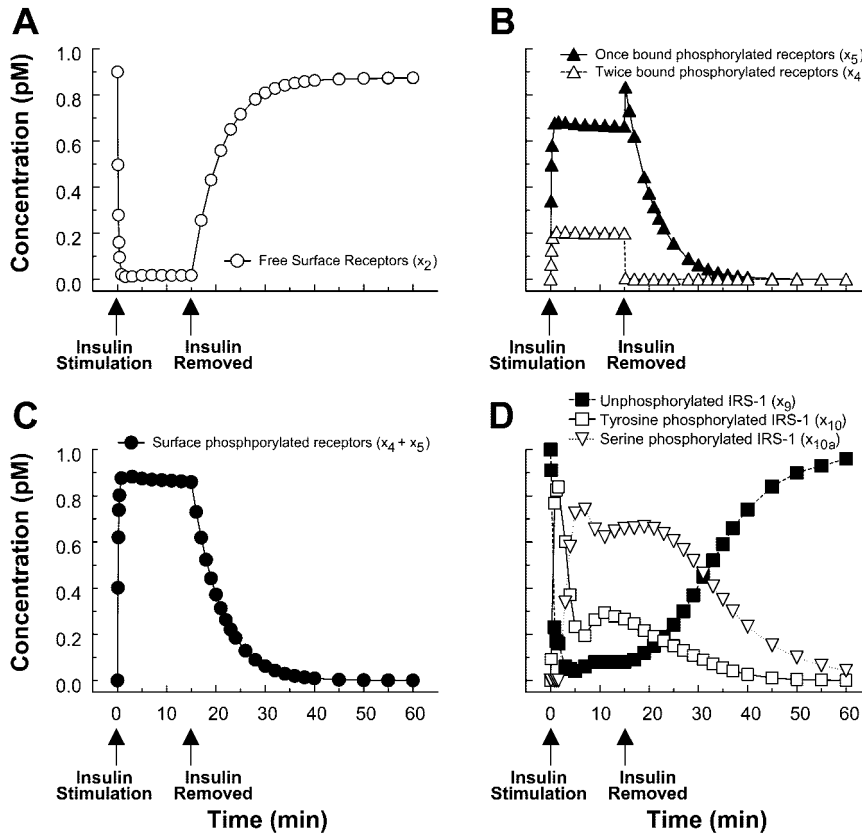
Fig. 8. Model simulations with feedback. Time courses for unbound receptors (*A*), once- and twice-bound phosphorylated surface receptors (*B*), total phosphorylated surface receptors (*C*), and unphosphorylated, serine-phosphorylated, and tyrosine-phosphorylated IRS-1 (*D*) after a step input of 10^{-7} M insulin for 15 min.

Fig. 9. Model simulations with feedback. Time courses for activated PI 3-kinase (*A*), levels of PI(3,4,5)P$_3$ and PI(3,4)P$_2$ (*B*), activated PKC-ζ (*C*), and cell surface GLUT4 (*D*) after a step input of 10^{-7} M insulin for 15 min.
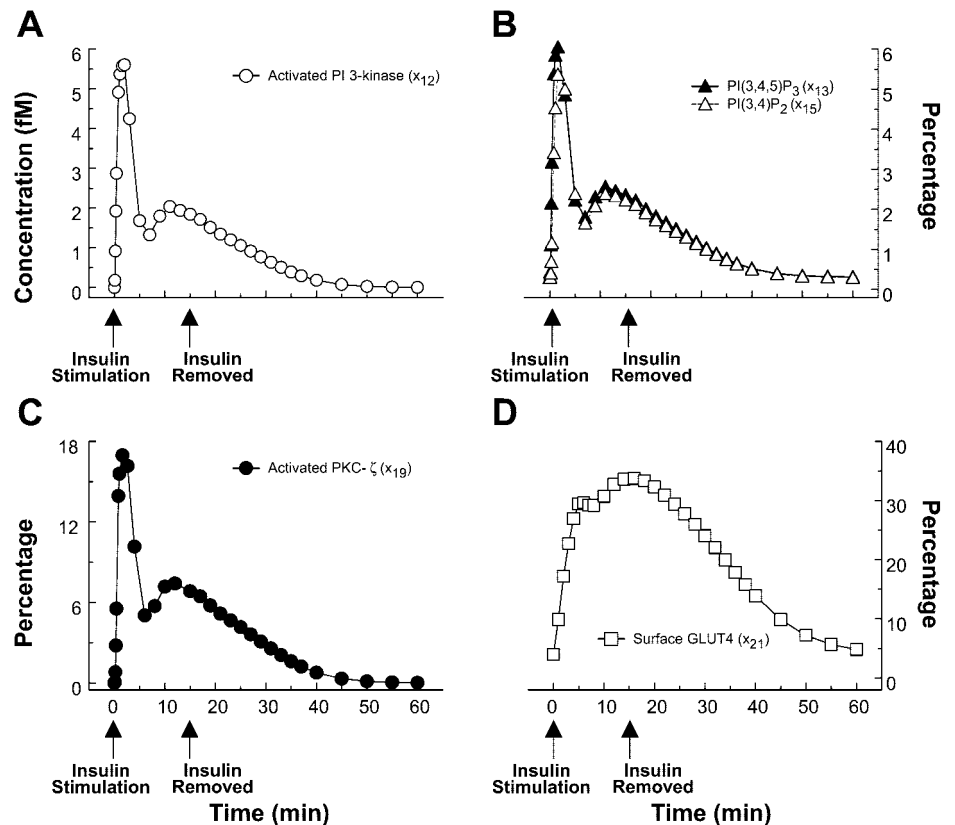
min. On removal of insulin, the concentration of activated PI 3-kinase returned to basal levels (time to half-maximal levels was ~17 min). The time courses for PI(3,4,5)P_3, PI(3,4)P_2, PKC-ζ, and Akt displayed a qualitatively similar dynamic (Fig. 9, *B* and *C*). That is, after 1 min of insulin stimulation, the level of PI(3,4,5)P_3 increased from 0.31% of the total lipid population to a peak of ~6.1% followed by an undershoot before equilibration at ~2.5%. The level of PI(3,4)P_2 increased from 0.21% to a peak of ~5.6% before equilibrating at a steady-state level of ~2.4%. On removal of insulin, both PI(3,4,5)P_3 and PI(3,4)P_2 returned to their basal levels (time to half-maximal levels was ~17 min). In response to insulin, the percentage of activated PKC-ζ transiently peaked at ~17.1% after ~1.5 min followed by an undershoot and equilibration at ~7.4% by 11 min. After insulin was removed, the level of activated PKC-ζ declined to basal levels with a time to half-maximal levels of ~17 min. Because we modeled the behavior of Akt identically to PKC-ζ, the time course for phosphorylated, activated Akt mirrored that for PKC-ζ (data not shown). With respect to translocation of GLUT4, the overall shapes of the time courses for cell surface GLUT4 with and without feedback were similar. However, with inclusion of positive and negative feedback loops, described above, the half-time for translocation of GLUT4 to the cell surface in response to insulin was slightly shorter than that observed in the model without feedback (~2.5 min), whereas the time for return to basal levels after insulin removal was longer (time to half-maximal level was ~18 min). Thus the inclusion of positive and negative feedback loops into our model of metabolic insulin signaling

generates predictions regarding the dynamics of various signaling components that may be experimentally testable.

Insulin Dose-Response Characteristics

We generated simulations of insulin dose-response curves to further explore characteristics of our model with and without feedback. Step inputs ranging from 10^{-6} to 10^{-12} M insulin for 15 min were used to construct dose-response curves for maximum levels of bound insulin receptors at the cell surface, total phosphorylated receptors at the cell surface, activated PI3-kinase, and cell surface GLUT4 (Fig. 10). Published experimental data corresponding to each of these elements were then compared with simulation results. The experimental data used for comparison were obtained from a series of experiments performed in the same preparation of rat adipose cells (47). For bound surface insulin receptors ($x_3 + x_4 + x_5$), the dose-response curve generated by our model without feedback had a half-maximal effective dose (ED$_{50}$) of 3.5 nM (Fig. 10*A*). Our model with feedback generated a curve with an ED$_{50}$ of 2.9 nM. Both of these simulation results were similar to the experimentally determined ED$_{50}$ of 7 nM that was reported by Stagsted et al. (47). With respect to receptor autophosphorylation, model simulations without feedback generated a dose-response curve for surface phosphorylated receptors ($x_4 + x_5$) with an ED$_{50}$ of 3.5 nM (Fig. 10*B*). Model simulations with feedback generated a dose-response curve with an ED$_{50}$ of 2.9 nM. The experimentally determined ED$_{50}$ for receptor autophosphorylation was
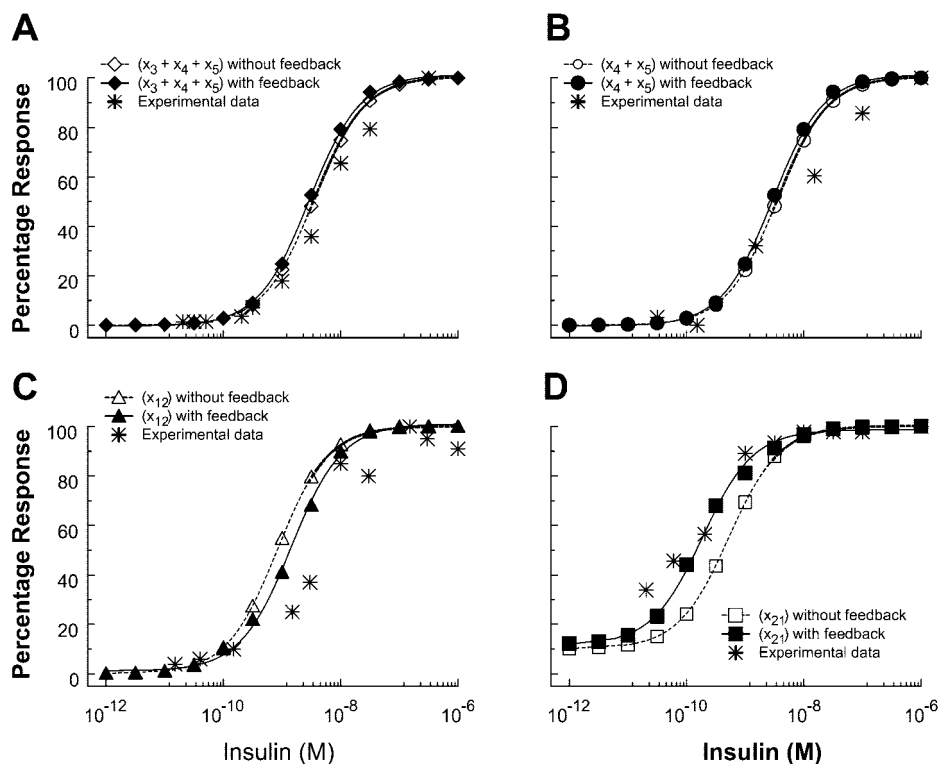

Fig. 10. Experimentally generated insulin dose-response curves adapted from Ref. 47 were compared with dose-response curves generated from our model with and without feedback for bound receptors (*A*), phosphorylated receptors at the cell surface (*B*), PI 3-kinase activity (*C*), and glucose uptake (*D*; assumed to be directly proportional to GLUT4 levels at the cell surface).

reported as 5 nM (47). The close similarity between insulin dose-response curves for receptor binding and receptor autophosphorylation observed in both our simulations and the experimental data is consistent with the tight coupling of the dynamics of these processes.

For activated PI 3-kinase, model simulations without feedback generated an insulin dose-response curve with an ED_{50} of 0.83 nM. Model simulations with feedback showed a slightly greater sensitivity with an ED_{50} of 1.43 nM. These simulation results seem reasonable, since downstream components should have greater insulin sensitivity than proximal events if one assumes that signal amplification occurs for downstream elements. Interestingly, the experimentally determined ED_{50} for activated PI 3-kinase reported by Stagsted et al. (47) is 8 nM. With respect to insulin-stimulated translocation of GLUT4, model simulations without feedback generated a dose-response curve with an ED_{50} of 0.53 nM, whereas model simulations with feedback generated a dose-response curve with a slightly smaller ED_{50} of 0.19 nM. In rat adipose cells, the ED_{50} = 0.17 nM for insulin-stimulated glucose uptake (47). Again, our simulation results are not only consistent with kinetic expectations but also closely match experimental results, including observations that maximal glucose uptake occurs with partial insulin receptor occupancy (47). A general result from these model simulations is that insulin sensitivity increases for components farther downstream in the signaling pathway. In addition, the presence of feedback in our model resulted in slightly increased sensitivity for each signaling component examined compared with simulations without feedback.

Biphasic Activation of PKC-ζ

Biphasic activation of PKC-ζ in rat adipocytes in response to insulin stimulation has been previously reported (48, 50). However, the mechanism underlying this dynamic is unknown. To determine whether the presence of feedback in insulin signaling pathways might account for this biphasic response, we compared published experimental data on activation of PKC-ζ with model simulations in the presence or absence of feedback. We used a step input of 10^{-8} M insulin for 15 min to mimic the experimental conditions reported in Standaert et al. (48). Intriguingly, the time course for activated PKC-ζ in response to insulin generated from the simulation with feedback displayed a biphasic dynamic that more closely matched the experimental data, whereas the model without feedback failed to produce a biphasic response (Fig. 11). Thus one possible mechanism to generate a biphasic activation of PKC-ζ in response to insulin is the presence of feedback pathways.

Effects of Increased Levels of PTPases on Insulin-Stimulated Translocation of GLUT4

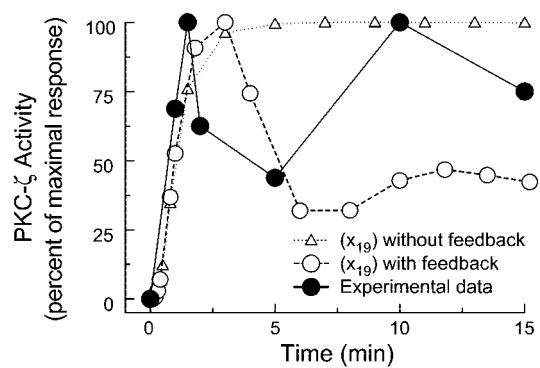To demonstrate the ability of our model to represent pathological conditions, we ran model simulations

Fig. 11. Biphasic activation of PKC-ζ in response to insulin stimulation. Published data on insulin-stimulated activation of PKC-ζ (adapted from Ref. 48, Fig. 2*A*; ●) were compared with simulation results from our model with (○) and without (△) feedback using a step input of 10^{-8} M insulin for 15 min.

without feedback where we examined the effects of increased PTPase activity on translocation of GLUT4. Simulations of the time courses for cell surface GLUT4 were generated for 15-min insulin step inputs of 10^{-7}, 10^{-9}, and 10^{-10} M and [PTP] = 1. These control curves were then compared with simulations in which [PTP] = 1.5 (mimicking diabetes or obesity). As might be predicted, increasing [PTP] resulted in a decreased amount of cell surface GLUT4 at every insulin dose and a more rapid return to the basal state when insulin is removed (Fig. 12). Moreover, the effect of increased PTPase activity to reduce cell surface GLUT4 (in terms of percentage) is more pronounced at lower insulin doses. Thus, at an insulin dose of 10^{-7} M, increasing [PTP] by 50% causes a 6.5% decrease in peak insulin-stimulated GLUT4 at the cell surface, whereas at the 10^{-10} M insulin dose, a 50% increase in [PTP] results in a 27.9% decrease in peak insulin-stimulated cell surface GLUT4. These results are consistent with the amplification properties of this signal transduction system and the function of PTPases to negatively regulate insulin signaling at the level of the insulin receptor and IRS-1. Model simulations with feedback gave qualitatively similar results (data not shown).

DISCUSSION

Since the discovery of insulin over 80 years ago, tremendous progress has been made in elucidating the molecular mechanisms of insulin action. However, recent investigations of insulin signaling reveal biological complexities that are still not fully understood. For example, the determinants of specificity for metabolic insulin signaling pathways are largely unknown. Rapid progress in the field of signal transduction and genomics has inspired the foundation of groups such as the National Resource for Cell Analysis and Modeling (NRCAM; pioneers in the Virtual Cell project; see Ref. 41) and The Alliance for Cellular Signaling. These groups strongly argue that a theoretical approach with a comprehensive database is absolutely necessary for a full understanding of cellular signaling behavior.
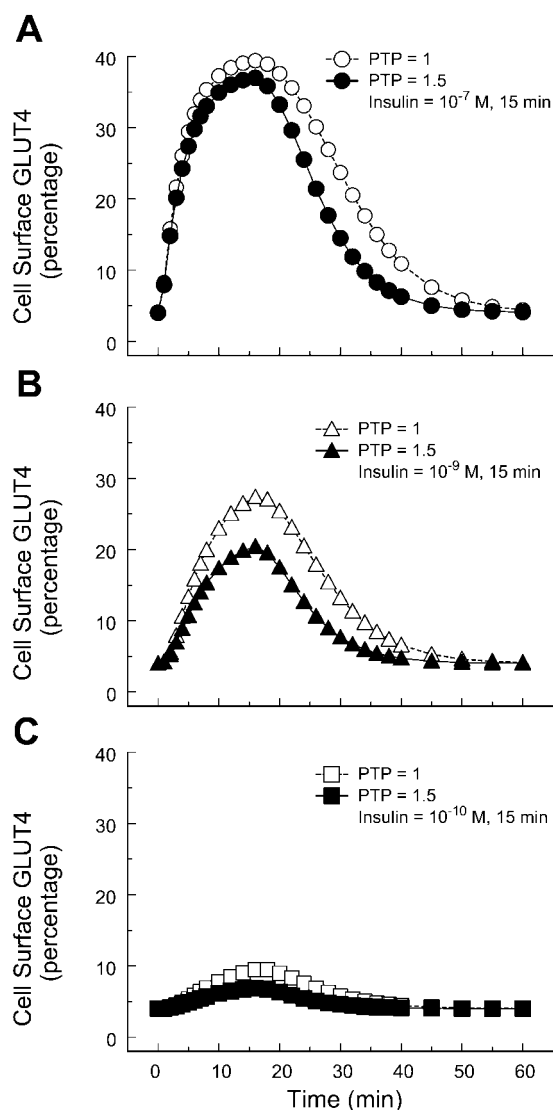
A

B

C

Fig. 12. Effects of increasing PTP on time courses for insulin-stimulated translocation of GLUT4. Simulations for cell surface GLUT4 in response to a 15-min step input of 10^{-7} M insulin (*A*), 10^{-9} M insulin (*B*), and 10^{-10} M insulin (*C*) are shown for [PTP] = 1.0 (open symbols) and [PTP] = 1.5 (solid symbols) using our model without feedback.

Model Development

Previous applications of mathematical modeling to insulin action have focused on limited areas such as receptor binding kinetics and GLUT4 trafficking (17, 35–37, 43, 44, 57). The predictive power of these models has been useful for understanding particular aspects of insulin action. In the present work, we incorporate some of these models along with a novel current description of insulin signal transduction elements into a complete model of metabolic insulin signaling pathways. Because some signaling elements represented in the model have just recently been discovered, biochemical characterization of the kinetics for these elements remains incomplete. For example, time courses of activation are often reported with reference to insulin stimulation without characterization relative to immediate upstream precursors. Moreover, limitations in experimental approaches preclude the determination of some time courses with sufficient resolution. Thus we did not explicitly include an element for PDK-1 between the generation of PI(3,4,5)P_3 and the phosphorylation of PKC-ζ and Akt because insufficient kinetic data are available in the literature. Similarly, elements downstream from PKC-ζ and Akt that link metabolic insulin signaling pathways with the machinery for GLUT4 trafficking are unknown and therefore not explicitly represented.

One potential pitfall in developing such a complicated model is that the number of arbitrary free parameter choices may decrease the predictive power of the model. To address this issue, we incorporated previous models as subsystems in our complete model to significantly reduce the number of arbitrary elements. Rate constants and parameters for these subsystems had previously been independently obtained and validated. The majority of remaining model parameters and rate constants characterizing newly modeled steps of the metabolic insulin signaling pathway were based on experimental data in the literature. We also used boundary value conditions to derive fixed relationships among various rate constants and model parameters to further decrease the degrees of freedom in the structure of the model. Finally, as a simplifying measure, we represented the numerous kinetic reactions in our model as first-order reactions coupled by shared common elements. We have attempted to thoroughly validate our complete model by demonstrating that the behavior of each individual state variable in response to a step insulin input closely matches experimental data from a variety of independent sources. As further evidence of the validity of our complete model, our system as a whole generated properties that have been observed experimentally, including the presence of "spare receptors" (e.g., maximal activation of GLUT4 translocation with submaximal insulin receptor occupancy), signal amplification, and increased insulin sensitivity for downstream components in the signaling pathway. Because three of the four model subsystems have previously been validated and the behavior of the overall model agrees closely with published experimental data, we conclude that our postreceptor signaling subsystem is reasonable and robust. Moreover, the rate constants chosen for the signaling subsystem were based on data in the literature. Although a more complete exploration of the postreceptor signaling subsystem is of interest, this is beyond the scope of the current study.

In some cases where mechanisms regulating interactions between signaling elements are not fully understood, we modeled these interactions as linear relationships. The rate of IRS-1 phosphorylation in response to activated insulin receptors, the rate of PI(3,4,5)P_3 generation in response to activated PI 3-kinase, the rate of PKC-ζ and Akt phosphorylation in response to

increased levels of $PI(3,4,5)P_3$, and the rate of exocytosis for GLUT4 in response to phosphorylated PKC-ζ and Akt are all modeled as simple linear functions. In the case of the negative feedback loop where PKC-ζ phosphorylates IRS-1 on serine residues, we modulated the rate constant for serine phosphorylation of IRS-1 using a standard Hill equation to incorporate a reasonable time lag. Importantly, we observed a good overall match between experimental data and model simulations for both insulin dose-response curves and time courses. Thus our coupling assumptions seem reasonable. Nevertheless, these points in the model represent areas that could be further refined in the future when a greater understanding of the molecular mechanisms involved is achieved. Indeed, by modeling more complicated coupling mechanisms, specific simulation results may give rise to experimentally testable predictions. This interplay between theoretical predictions and experimental results may yield important insights into the molecular mechanisms of insulin action.

Model Simulations without Feedback

We validated the structure of our complete model by comparing published experimental data with model simulations in response to an acute insulin stimulus. In our model without feedback, the dynamics of insulin-stimulated phosphorylation of IRS-1, activation of PI 3-kinase, production of $PI(3,4,5)P_3$ and $PI(3,4)P_2$, and phosphorylation of Akt and PKC-ζ all fit well with published experimental data (2, 29, 46, 48, 55). On removal of insulin, the dynamics of the return to basal states in our simulations showed a time to half-maximal levels of ~8 min for phosphorylated IRS-1 and activated PI 3-kinase and ~11 min for $PI(3,4,5)P_3$, phosphorylated Akt, and phosphorylated PKC-ζ. Because minimal kinetic data exist regarding the return to basal levels after removal of insulin, these simulation results represent predictions of our model. Finally, as expected, time courses for insulin receptor binding and GLUT4 translocation also matched experimental data when these subsystems were placed into the context of the overall model.

In our simulations we observed a time lag between the insulin input and subsequent steps in insulin signaling that increased as the signal propagated downstream. This lag was present for simulations of both insulin stimulation and removal. Because the kinetics governing most state variables were modeled as first-order events, recovery to basal conditions of each component would be expected to appear as a concave-up, exponential decay curve. Interestingly, in our simulations of insulin removal (after 15-min insulin stimulation), we observed the presence of a concave-down region immediately before the concave-up exponential decay that became more pronounced for distal components and is clearly evident in the simulations of GLUT4 translocation (Fig. 7D). This qualitative behavior is consistent with the presence of a signaling cascade that controls insulin-stimulated translocation of GLUT4 and has been observed experimentally in rat adipose cells (20).

To further validate our complete model without feedback, we compared published experimental data with simulations of insulin dose-response curves for key state variables (Fig. 10). The usefulness of these comparisons was substantially strengthened by the fact that data on insulin receptor binding, receptor autophosphorylation, PI 3-kinase activation, and glucose transport were obtained from a single experimental preparation of rat adipose cells (47). Qualitatively, the sigmoidal shape of dose-response curves generated by our model simulations (when plotted as a semi-log graph) is consistent with the hyperbolic response characteristic of most receptor-mediated biological events. In addition, we observed increased insulin sensitivity for downstream components of the insulin signaling pathway. That is, $ED_{50} = 3.5$ nM for receptor binding, $ED_{50} = 3.5$ nM for receptor autophosphorylation, $ED_{50} = 0.83$ nM for PI 3-kinase activation, and $ED_{50} = 0.53$ nM for GLUT4 translocation. This increased sensitivity of downstream components, consistent with the presence of a signal amplification cascade, is a well-described characteristic for biological actions of insulin. For example, only a fraction of insulin receptors need to be occupied by insulin for maximal glucose uptake to occur in adipose cells (20, 47). Stagsted et al. (47) reported an ED_{50} of 8 nM for insulin-stimulated PI 3-kinase activation. However, close inspection of their data suggests that the actual value may be closer to 4 nM. Nevertheless, this ED_{50} is still somewhat larger than the ED_{50} of 0.83 nM derived from our simulations. However, the measurement of PI 3-kinase activity in anti-phosphotyrosine immunoprecipitates derived from whole cell lysates is difficult to perform in a quantitative manner. Thus it is possible that the small discrepancy between our simulation results and experimental data with respect to activation of PI3-kinase may be explained, in part, by imprecision introduced by experimental variability. Of note, the shape and ED_{50} of insulin dose-response curves for insulin receptor binding, receptor autophosphorylation, and GLUT4 translocation almost exactly match the corresponding experimentally determined dose-response curves (Fig. 10). Thus the insulin sensitivity of key components of our model is realistic. Moreover, given the fact that our model structure, rate constants, and parameters were derived from a large mixture of many different experimental systems, this remarkable fit to experimental data from a single system across several key state variables suggests that the overall structure of our model is quite robust.

Model Simulations with Feedback

To further explore the complexities of insulin signaling, we simultaneously modeled positive and negative feedback loops based on mechanisms proposed in the literature (9, 33, 38, 39). We incorporated a positive

feedback loop into our model by having Akt phosphorylate PTP1B and impair its ability to dephosphorylate the insulin receptor and IRS-1 (38). The slight increase in insulin sensitivity for insulin binding and receptor autophosphorylation observed in our model with feedback was an expected result of positive feedback at the level of the insulin receptor. That is, decreased activity of PTPases against phosphorylated insulin receptors results in subtle shifts in the equilibrium states for the various receptor state variables. Similarly, we observed slightly decreased sensitivity for the activated PI 3-kinase dose-response curve derived from our model with feedback. This is the result of positive feedback with Akt phosphorylating PTP1B and inhibiting tyrosine dephosphorylation of IRS-1. In addition, the lower equilibrium level of PI 3-kinase after maximal insulin stimulation (which defines the parameter PI3K) also contributes to a shift in insulin sensitivity at the level of PI 3-kinase. Dose-response curves for translocation of surface GLUT4 derived from the model with feedback demonstrated greater insulin sensitivity than simulations without feedback. This was due to the combined effects of increased sensitivity of proximal signaling elements. Remarkably, the experimental data for insulin-stimulated glucose uptake reported by Stagsted et al. (47) indicated an ED_{50} of 1.7 nM that almost exactly matched the ED_{50} of 1.9 nM for cell surface GLUT4 that we calculated from our model with feedback. In addition to slightly increased insulin sensitivity, the half-times for return to basal levels of all signaling elements were longer in our simulations with feedback. These results are consistent with experimental observations suggesting that positive feedback at the level of the insulin receptor and IRS-1 slows the return of activated signaling elements to basal levels (38).

We incorporated a negative feedback loop into our model by modeling the ability of PKC-ζ to phosphorylate IRS-1 on serine residues and impair its ability to bind and activate PI 3-kinase (39). Time courses for insulin receptor binding and phosphorylation generated by models with and without feedback were similar. However, the overall dynamics of postreceptor signaling elements in our model were quite different with inclusion of feedback. In response to insulin stimulation, we observed a transient damped oscillatory behavior before equilibrium was reached in all elements of the postreceptor signaling subsystem. This oscillatory behavior was a direct result of negative feedback by PKC-ζ. Immediately after insulin stimulation, effects of PKC-ζ on upstream components are not apparent because of the time lag present for distal signaling components. As levels of phosphorylated PKC-ζ increase (and the value of parameter [PKC] approaches 1), the rate constant for serine phosphorylation of IRS-1 increases, resulting in depletion of the tyrosine-phosphorylated IRS-1 pool. As biochemical reactions within the postreceptor signaling pathway shift and react to effects of this negative feedback, time courses of postreceptor elements exhibit a transient oscillatory behavior before a final equilibrium state is reached. Although this qualitative behavior has not been re-

ported for insulin-stimulated PI 3-kinase activity, it is possible that time courses with sufficiently fine resolution to capture this behavior have not been performed. Intriguingly, a damped oscillatory behavior or biphasic activation of PKC-ζ in response to insulin stimulation previously has been reported in several studies (48, 50). Only our model with feedback (but not without feedback) generated simulations for insulin-stimulated PKC-ζ activity that closely matched the complex dynamic for PKC-ζ present in published experimental data (48). Thus one novel result from our model is the suggestion that negative feedback from PKC-ζ to IRS-1 may be sufficient to explain the complex dynamic behavior of PKC-ζ activity in response to insulin.

Modeling Increased Levels of PTPases

In addition to giving insight into normal physiology, our model may also be useful for helping to understand pathological conditions. Diabetes is a disease characterized by insulin resistance that may be related, in part, to elevated levels of protein tyrosine phosphatases such as PTP1B (15). We simulated a pathological condition where activity of PTPases was 50% above normal ([PTP] = 1.5). Over a range of insulin doses, this was associated with a decrease in peak cell surface GLUT4 compared with simulations where [PTP] = 1. The percent decrease in peak GLUT4 was greater for lower insulin doses, and the half-times for recovery to basal conditions were significantly shortened by increasing [PTP]. Similar effects were observed in the models with and without feedback. Thus our model can make specific predictions about the nature of insulin resistance due to increased levels of PTPases such as PTP1B. Similarly, it may be possible to explore mechanisms of insulin resistance due to altered lipid phosphatase function by manipulation of the parameters [SHIP] and [PTEN].

In conclusion, the mathematical model of metabolic insulin signaling pathways developed here is based on previous subsystem models as well as new elements characterizing the molecular mechanisms of insulin signaling. The model structure was extensively validated and sufficient to explain qualitative behaviors that are experimentally observed in both normal and pathological states. In addition, our model with feedback suggests a potential mechanistic explanation for the damped oscillatory behavior of PKC-ζ activity in response to insulin that is observed experimentally. Moreover, various mechanisms used to couple model subsystems represent experimentally testable hypotheses. Consequently, we hope that our model will be a useful predictive tool for generating hypotheses to complement and motivate experimental approaches. This may lead to a better understanding of the normal physiology of insulin action as well as the pathophysiology underlying insulin resistance that contributes to major public health problems such as diabetes and obesity.

APPENDIX A

Model without Feedback

State variables are as follows

x_1 = Insulin input
x_2 = Concentration of unbound surface insulin receptors
x_3 = Concentration of unphosphorylated once-bound surface receptors
x_4 = Concentration of phosphorylated twice-bound surface receptors
x_5 = Concentration of phosphorylated once-bound surface receptors
x_6 = Concentration of unbound unphosphorylated intracellular receptors
x_7 = Concentration of phosphorylated twice-bound intracellular receptors
x_8 = Concentration of phosphorylated once-bound intracellular receptors
x_9 = Concentration of unphosphorylated IRS-1
x_{10} = Concentration of tyrosine-phosphorylated IRS-1
x_{11} = Concentration of unactivated PI 3-kinase
x_{12} = Concentration of tyrosine-phosphorylated IRS-1/activated PI 3-kinase complex
x_{13} = Percentage of PI(3,4,5)P$_3$ out of the total lipid population
x_{14} = Percentage of PI(4,5)P$_2$ out of the total lipid population
x_{15} = Percentage of PI(3,4)P$_2$ out of the total lipid population
x_{16} = Percentage of unactivated Akt
x_{17} = Percentage of activated Akt
x_{18} = Percentage of unactivated PKC-ζ
x_{19} = Percentage of activated PKC-ζ
x_{20} = Percentage of intracellular GLUT4
x_{21} = Percentage of cell surface GLUT4

Equations are as follows

x_1 = insulin input
$dx_2/dt = k_{-1}x_3 + k_{-3}[\text{PTP}]x_5 - k_1x_1x_2 + k_{-4}x_6 - k_4x_2$
$dx_3/dt = k_1x_1x_2 - k_{-1}x_3 - k_3x_3$
$dx_4/dt = k_2x_1x_5 - k_{-2}x_4 + k_{-4'}x_7 - k_{4'}x_4$
$dx_5/dt = k_3x_3 + k_{-2}x_4 - k_2x_1x_5 - k_{-3}[\text{PTP}]x_5 + k_{-4'}x_8 - k_{4'}x_5$
$dx_6/dt = k_5 - k_{-5}x_6 + k_6[\text{PTP}](x_7 + x_8) + k_4x_2 - k_{-4}x_6$
$dx_7/dt = k_{4'}x_4 - k_{-4'}x_7 - k_6[\text{PTP}]x_7$
$dx_8/dt = k_{4'}x_5 - k_{-4'}x_8 - k_6[\text{PTP}]x_8$
$dx_9/dt = k_{-7}[\text{PTP}]x_{10} - k_7x_9(x_4 + x_5)/(\text{IR}_\text{p})$
$dx_{10}/dt = k_7x_9(x_4 + x_5)/(\text{IR}_\text{p}) + k_{-8}x_{12} - (k_{-7}[\text{PTP}] + k_8x_{11})x_{10}$
$dx_{11}/dt = k_{-8}x_{12} - k_8x_{10}x_{11}$
$dx_{12}/dt = k_8x_{10}x_{11} - k_{-8}x_{12}$
$dx_{13}/dt = k_9x_{14} + k_{10}x_{15} - (k_{-9}[\text{PTEN}] + k_{-10}[\text{SHIP}])x_{13}$
$dx_{14}/dt = k_{-9}[\text{PTEN}]x_{13} - k_9x_{14}$
$dx_{15}/dt = k_{-10}[\text{SHIP}]x_{13} - k_{10}x_{15}$
$dx_{16}/dt = k_{-11}x_{17} - k_{11}x_{16}$
$dx_{17}/dt = k_{11}x_{16} - k_{-11}x_{17}$
$dx_{18}/dt = k_{-12}x_{19} - k_{12}x_{18}$
$dx_{19}/dt = k_{12}x_{18} - k_{-12}x_{19}$
$dx_{20}/dt = k_{-13}x_{21} - (k_{13} + k_{13'})x_{20} + k_{14} - k_{-14}x_{20}$
$dx_{21}/dt = (k_{13} + k_{13'})x_{20} - k_{-13}x_{21}$

Initial conditions are as follows

$x_1(0) = 0$
$x_2(0) = 9 \times 10^{-13}$ M
$x_3(0) = 0$
$x_4(0) = 0$
$x_5(0) = 0$
$x_6(0) = 1 \times 10^{-13}$ M
$x_7(0) = 0$
$x_8(0) = 0$
$x_9(0) = 1 \times 10^{-12}$ M
$x_{10}(0) = 0$
$x_{11}(0) = 1 \times 10^{-13}$ M
$x_{12}(0) = 0$
$x_{13}(0) = 0.31\%$
$x_{14}(0) = 99.4\%$
$x_{15}(0) = 0.29\%$
$x_{16}(0) = 100\%$
$x_{17}(0) = 0$
$x_{18}(0) = 100\%$
$x_{19}(0) = 0$
$x_{20}(0) = 96\%$
$x_{21}(0) = 4\%$

Model parameters are as follows

$k_1 = 6 \times 10^7$ M$^{-1}\cdot$min^{-1}
$k_{-1} = 0.20$ min^{-1}
$k_2 = k_1$
$k_{-2} = 100k_{-1}$
$k_3 = 2{,}500$ min^{-1}
$k_{-3} = k_{-1}$
$k_4 = k_{-4}/9$
$k_{-4} = 0.003$ min^{-1}
$k_{4'} = 2.1 \times 10^{-3}\cdot$min^{-1}
$k_{-4'} = 2.1 \times 10^{-4}\cdot$min^{-1}
$k_5 = 10k_{-5}$ M$\cdot$min^{-1} if $(x_6 + x_7 + x_8) > 1 \times 10^{-13}$
  $= 60k_{-5}$ M$\cdot$min^{-1} if $(x_6 + x_7 + x_8) \leq 1 \times 10^{-13}$
$k_{-5} = 1.67 \times 10^{-18}$ min^{-1}
$k_6 = 0.461$ min^{-1}
$k_7 = 4.16$ min^{-1}
$k_{-7} = (2.5/7.45)k_7$
$k_8 = k_{-8}(5/70.775) \times 10^{12}$
$k_{-8} = 10$ min^{-1}
$k_9 = (k_{9(\text{stimulated})} - k_{9(\text{basal})})(x_{12}/\text{PI3K}) + k_{9(\text{basal})}$
$k_{9(\text{stimulated})} = 1.39$ min^{-1}
$k_{-9} = (94/3.1)k_{9(\text{stimulated})}$
$k_{9(\text{basal})} = (0.31/99.4)k_{-9}$
$k_{10} = (3.1/2.9)k_{-10}$
$k_{-10} = 2.77$ min^{-1}
$k_{11} = (0.1k_{-11})(x_{13} - 0.31)/(3.10 - 0.31)$
$k_{-11} = 10 \ln (2)$ min^{-1}
$k_{12} = (0.1k_{-12})(x_{13} - 0.31)/(3.10 - 0.31)$
$k_{-12} = 10 \ln (2)$ min^{-1}
$k_{-13} = 0.167$ min^{-1}
$k_{13} = (4/96)k_{-13}$
$k_{13'} = [(40/60) - (4/96)]k_{-13}\cdot(\text{Effect})$
$k_{14} = 96k_{-14}$
$k_{-14} = 0.001155$ min^{-1}
effect $= (0.2x_{17} + 0.8x_{19})/(\text{AP}_\text{equil})$
IR$_\text{p} = 8.97 \times 10^{-13}$ M
[SHIP] $= 1.00$
[PTEN] $= 1.00$
[PTP] $= 1.00$
AP$_\text{equil} = 100/11$
PI3K $= 5 \times 10^{-15}$ M

Model with Feedback

Additional state variables are as follows

$x_{10\text{a}}$ = concentration of serine-phosphorylated IRS-1

Additional equations are as follows

$$dx_9/dt = k_{-7}[PTP]x_{10} - k_7 x_9(x_4 + x_5)/(IR_p) + k_{-7'}x_{10a} - k_{7'}[PKC]x_9 \text{ (updated)}$$
$$dx_{10a}/dt = k_7[PKC]x_9 - k_{-7'}x_{10a}$$

Additional initial conditions are as follows

$$x_{10a}(0) = 0$$

Additional parameters are as follows

$$k_{7'} = \ln(2)/2 \text{ min}^{-1}$$
$$k_{-7'} = k_{7'} [(2.5/7.45)(3.70 \times 10^{-13})]/[(6.27 \times 10^{-13}) - (2.5/7.45)(3.70 \times 10^{-13})]$$
$$[PTP] = 1.00 [1 - 0.25(x_{17}/(100/11)] \text{ for } x_{17} \leq (400/11),$$
$$\text{otherwise } [PTP] = 0 \text{ (updated)}$$
$$PI3K = k_8(3.70 \times 10^{-13})(1 \times 10^{-13})/[k_8(3.70 \times 10^{-13}) + k_{-8}] \text{ (updated)}$$
$$[PKC] = V_{max}x_{19}(t - \tau)^n/[K_d^n + x_{19}(t - \tau)^n]$$
$$V_{max} = 20$$
$$K_d = 12$$
$$n = 4$$
$$\tau = 1.5$$

APPENDIX B

Initial Conditions, Rate Constants, and Parameter Choice for Complete Model without Feedback

Where possible, initial conditions and model parameters were determined by known boundary value conditions or experimental data as previously described (35–37, 57). Table 1 lists initial conditions for the basal state (no insulin) of state variables obtained from previous models. Initial conditions for x_4, x_5, x_7, and x_8 were set to zero because, in the absence of insulin, we assumed that no receptors are bound to insulin. Similarly, initial basal conditions for phosphorylated IRS-1, phosphorylated IRS-1/activated PI 3-kinase complex, and phosphorylated Akt and PKC-ζ (x_{10}, x_{12}, x_{17}, and x_{19}) were set to zero. The initial concentration for unphosphorylated IRS-1 (x_9) was set to 10^{-12} M on the basis of experimental results from 3T3-L1 adipocytes (21, 29). From published concentrations of purified PI 3-kinase obtained from rat liver and an estimate of the efficiency of purification (4, 25), we set the basal intracellular PI 3-kinase concentration (x_{11}) at 10^{-13} M. Under basal conditions, the percentage distribution of PI(3,4,5)P$_3$ (x_{13}), PI(4,5)P$_2$ (x_{14}), and PI(3,4)P$_2$ (x_{15}) in COS-7 cells is 0.31, 99.4, and 0.29%, respectively, of the total pool (23). Therefore, we used these values for the initial basal conditions of x_{13}, x_{14}, and x_{15}. We assumed that neither Akt nor PKC-ζ is in the phosphorylated, activated state under basal conditions. Thus we set initial conditions for unphosphorylated Akt (x_{16}) and unphosphorylated PKC-ζ (x_{18}) equal to 100% of the amount of these proteins in the cell. We represented these state variables in terms of percentages

Table 1. *Initial conditions obtained from previously validated subsystem models*

Subsystem Model	Initial Conditions
Insulin binding kinetics (57)	$x_2(0) = 9 \times 10^{-13}$ M
	$x_3(0) = 0$ M
Insulin receptor recycling (36)	$x_6(0) = 1 \times 10^{-13}$ M
GLUT4 translocation (35, 37)	$x_{20}(0) = 96\%$
	$x_{21}(0) = 4\%$

Nos. in parentheses refer to references.

Table 2. *Rate constants obtained from previously validated subsystem models*

Subsystem Model	Rate Constants
Insulin binding kinetics (57)	$k_1 = 6 \times 10^7$ M$^{-1}\cdot$min^{-1}
	$k_{-1} = 0.20$ min^{-1}
	$k_2 = k_1$
	$k_{-2} = 100k_{-1}$
Insulin receptor recycling (36)	$k_4 = 0.003$ min^{-1}
	$k_{-4} = k_4/9$
	$k_5 = 10k_{-5}$ M$^{-1}\cdot$min^{-1} if $(x_6 + x_7 + x_8) > 1 \times 10^{-13}$
	$= 60k_{-5}$ M$^{-1}\cdot$min^{-1} if $(x_6 + x_7 + x_8) \leq 1 \times 10^{-13}$
	$k_{-5} = 1.67 \times 10^{-18}$ min^{-1}
GLUT4 translocation (35, 37)	$k_{-13} = 0.167$ min^{-1}
	$k_{14} = 96k_{-14}$ M$^{-1}\cdot$min^{-1}
	$k_{-14} = 0.001155$ min^{-1}

because we could not find published estimates of cellular concentrations for either Akt or PKC-ζ.

Table 2 lists values for rate constants obtained from previous subsystem models. For the rate constant for insulin receptor autophosphorylation (k_3), we chose a value of 2,500 min^{-1} that was determined experimentally in vitro (1). This is consistent with the rapid autophosphorylation of insulin receptors in intact cells (44, 58, 59). For the rate constant governing receptor dephosphorylation (k_{-3}), we assumed that release of insulin from the insulin receptor was rate limiting and that receptors were immediately dephosphorylated once they returned to the basal unoccupied state (11, 30, 31, 44). Therefore, we chose $k_{-3} = k_{-1}$. The rate constant for phosphorylated receptor endocytosis ($k_{4'}$) was chosen to be 2.1×10^{-3} min^{-1}. This is the value used for the endocytosis rate constant for bound insulin receptors in our previous model (36). Because the rate of ligand-mediated endocytosis exceeds the rate for exocytosis, we chose a ratio of endocytosis and exocytosis rate constants for phosphorylated receptors of 10:1 so that $k_{-4'} = 2.1 \times 10^{-4}$ min^{-1}. When phosphorylated receptors are internalized, insulin dissociates and receptors undergo rapid dephosphorylation. The half-time for internalized receptor dephosphorylation (after maximal phosphorylation by insulin stimulation) is ~1.5 min in rat liver endosomes (11). For a first-order rate constant

$$k = [\ln(2)]/(t_{1/2}) \tag{B32}$$

Therefore, assuming half-time ($t_{1/2}$) = 1.5 min for internalized receptor dephosphorylation, the rate constant for intracellular receptor dephosphorylation (k_6) is 0.461 min^{-1}.

For reactions in the postreceptor signaling subsystem, the choice of rate constants was based on experimental data where possible. To further limit the number of free parameters, we also used published data to derive fixed relationships among various rate constants. On maximal insulin stimulation, most IRS-1 is tyrosine phosphorylated (52) with a half-time of ~10 s in 3T3-L1 adipocytes (29). Under these conditions, ~5% of PI 3-kinase is activated in Fao cells (16). By using initial conditions described in APPENDIX A for the basal state and assuming that 75% of all IRS-1 becomes tyrosine phosphorylated with maximal insulin stimulation, equilibrium values for x_9 through x_{12} after maximal insulin stimulation will be $x_9 = 2.5 \times 10^{-13}$ M, $x_{10} = 7.45 \times 10^{-13}$ M, $x_{11} = 9.5 \times 10^{-14}$ M, and $x_{12} = 5.0 \times 10^{-15}$ M. By assuming the

half-time for maximal IRS-1 phosphorylation to be 10 s, $k_7 =$ 4.16 min^{-1} (using *Eq. 32*). Under normal physiological conditions, where PTP = 1, *Eq. 14* can be simplified and rearranged as $k_{-7} = (x_9/x_{10})k_7$ in the equilibrium state after maximal insulin stimulation. Thus, under conditions of maximal insulin stimulation, $k_{-7} = (2.5/7.45)k_7$. Reassuringly, these values for k_7 and k_{-7} are consistent with the time course for IRS-1 phosphorylation and dephosphorylation observed in rat adipose cells (24). Similarly, at equilibrium, *Eqs. 16* and *17* can be simplified and rearranged as $k_8 = x_{12}/(x_{10} x_{11})k_{-8}$. Because we were unable to find data on rates for association or dissociation of IRS-1 with PI 3-kinase, we chose $k_{-8} = 10 min^{-1}$ to be consistent with the scale of other rate constants in the postreceptor signaling subsystem. Thus, at maximal insulin stimulation, we constrained $k_8 = (50/70.775) \times 10^{12} M^{-1} \cdot min^{-1}$.

On the basis of data from 3T3-L1 cells, we assumed that levels for both $PI(3,4,5)P_3$ and $PI(3,4)P_2$ rise 10-fold after maximal insulin stimulation (22, 46), resulting in a new equilibrium distribution of 3.1, 94, and 2.9% for $PI(3,4,5)P_3$, $PI(4,5)P_2$, and $PI(3,4)P_2$, respectively. Because insulin-stimulated conversion of $PI(4,5)P_2$ to $PI(3,4,5)P_3$ is mediated by the phosphorylated IRS-1/activated PI 3-kinase complex, there is an increase in the rate constant governing this process (k_9) with insulin stimulation. We represented the transition in k_9 from the basal value [$k_{9(basal)}$] to the insulin-stimulated value [$k_{9(stimulated)}$] as a linear function of activated PI 3-kinase present in the cell

$$k_9 = [k_{9(stimulated)} - k_{9(basal)}](x_{12}/PI3K) + k_{9(basal)} \quad (B33)$$

where PI3K is the equilibrium concentration of activated PI 3-kinase obtained after maximal insulin stimulation. Data from 3T3-L1 preadipocytes suggest that conversion of $PI(4,5)P_2$ to $PI(3,4,5)P_3$ in response to insulin stimulation occurs with a half-time of ~30 s (when a time lag from upstream signaling events is considered) (46). Assuming a 30-s half-time for conversion of $PI(4,5)P_2$ to $PI(3,4,5)P_2$ and using *Eq. 32*, we calculated $k_{9(stimulated)} = 1.39 min^{-1}$. For both basal and insulin-stimulated equilibrium states, *Eq. 19* can be simplified and rearranged to show that $k_9 = (x_{13}/x_{14})k_{-9}$ (under normal physiological conditions, where PTEN = 1). Therefore, k_{-9} and $k_{9(basal)}$ can be constrained: $k_{-9} = (94/3.1)k_{9(stimulated)}$ and $k_{9(basal)} = (0.31/99.4)k_{-9}$. Similarly, data from 3T3-L1 preadipocytes suggest that conversion of $PI(3,4,5)P_3$ to $PI(3,4)P_2$ occurs with a half-time of ~15 s (46). By assuming a 15-s half-time for conversion of $PI(3,4,5)P_3$ to $PI(3,4)P_2$, $k_{-10} = 2.77 min^{-1}$. For both basal and insulin-stimulated equilibrium states, *Eq. 20* can be simplified to constrain $k_{10} = (3.1/2.9)k_{-10}$ (under normal physiological conditions, where SHIP = 1).

To define kinetic rate constants for activation and deactivation of Akt and PKC-ζ, we used data from rat skeletal muscle cells and rat adipocytes showing that PKC-ζ and Akt are both activated by insulin at approximately the same rate and that both enzymes reach maximal activation within 5 min of insulin stimulation (48, 55). There are no published data on the time course of activation in intact cells for Akt or PKC-ζ by their immediate signaling precursors. However, experimental data suggest that after taking into account the time lag between insulin binding and generation of $PI(3,4,5)P_3$, the induced activation of Akt and PKC-ζ probably occurs within 2 min (50, 56). Thus we chose rate constants for Akt and PKC-ζ activation, k_{11} and k_{12}, to be the same and also assumed that the half-time for maximal Akt and PKC-ζ activation was 1 min. Thus, by using *Eq. 32*, $k_{11} = k_{12} = [ln(2)] min^{-1}$ at equilibrium after maximal insulin stimulation.

Because many other growth factors can activate Akt and PKC-ζ simultaneously (19, 28), we assumed that with maximal insulin stimulation, both Akt and PKC-ζ exist in a 10:1 unactivated-to-activated distribution at equilibrium. Therefore, from *Eqs. 21–24*, we can constrain $k_{-11} = 10k_{11} = 10 ln(2)$ and $k_{-12} = 10k_{12} = 10 ln(2)$. Because $PI(3,4,5)P_3$ formation mediates Akt and PKC-ζ activation (50, 56), we assumed that rate constants for activation of both Akt and PKC-ζ increase from zero to their maximal values as a linear function of the increase in $PI(3,4,5)P_3$ levels

$$k_{11} = (0.1k_{-11})(x_{13} - 0.31)/(3.10 - 0.31) \quad (B34)$$

$$k_{12} = (0.1k_{-12})(x_{13} - 0.31)/(3.10 - 0.31) \quad (B35)$$

where 0.31 is the basal value of $PI(3,4,5)P_3$ and 3.10 is the value of $PI(3,4,5)P_3$ in the cell after maximal insulin stimulation. The values used for k_{-13}, k_{14}, and k_{-14} were previously defined for the GLUT4 translocation subsystem (Table 2), and the values for k_{13} and $k_{13'}$ can be derived from this information using *Eqs. 28* and *29*.

The parameter [PTP] was defined as the relative activity of protein tyrosine phosphatases in the cell. Thus [PTP] = 1 under normal physiological conditions, whereas pathological variations in PTPase activity can be represented by altering [PTP]. Similarly, model parameters [SHIP] and [PTEN] were defined as the relative activity of 5' and 3' lipid phosphatases, respectively, in the cell ([SHIP] = 1 and [PTEN] = 1 under normal conditions). The value for IR_p (used in *Eqs. 14* and *15*) was determined to be 8.97×10^{-13} M, based on calculations using equilibrium conditions obtained during maximal insulin stimulation for *Eqs. 6–13* and assuming that receptor downregulation is negligible during acute insulin stimulation. The value for AP_equil (used in *Eq. 29*) was determined to be 100/11 (based on a 10:1 unactivated-to-activated distribution of both Akt and PKC-ζ). The value for PI3K (used in *Eq. B33*) was chosen as 5×10^{-15} M based on experimental data indicating that ~5% of PI 3-kinase is activated on maximal insulin stimulation (16).

Additional Initial Conditions, Rate Constants, and Parameter Choice for Complete Model with Feedback

We assume that there is no serine phosphorylation of IRS-1 in the absence of insulin stimulation. Therefore, we chose the initial value of $x_{10a} = 0$. In NIH-3T3^{IR} cells, the phosphotyrosine content of IRS-1 after maximal insulin stimulation decreases by ~50% at 60 min (39). Thus, with inclusion of this negative feedback circuit, we chose the insulin-stimulated equilibrium value of $x_{10} = 3.7 \times 10^{-13}$ M to reflect this 50% decrease. With the use of steady-state conditions for *Eq. 17* and initial conditions $x_{11} + x_{12} = 1 \times 10^{-13}$ M, the insulin-stimulated equilibrium level for x_{12} was calculated to be $k_8(3.70 \times 10^{-13})(1 \times 10^{-13})/[k_8(3.70 \times 10^{-13}) + k_{-8}] = 2.54 \times 10^{-15}$ M. Because the total amount of IRS-1 is constant ($x_9 + x_{10} + x_{10a} + x_{12}$), the insulin-stimulated equilibrium level of $x_9 + x_{10a} = 6.27 \times 10^{-13}$ M. Values for k_7, k_{-7}, k_8, and k_{-8} remained the same as for the model without feedback. We assumed the half-time for IRS-1 serine phosphorylation was 2 min. From *Eq. B32*, we calculated $k_{7'} = ln(2)/2 min^{-1}$. With the use of the parameter constraints and derived equilibrium concentrations described in APPENDIX A as well as *Eqs. 30* and *31*, $k_{-7'} = k_{7'}[(2.5/7.45)(3.70 \times 10^{-13})]/[(6.27 \times 10^{-13}) - (2.5/7.45)(3.70 \times 10^{-13})]$ at equilibrium after maximal insulin stimulation. Finally, to properly incorporate this negative feedback loop into our model, the factor PI3K from *Eq. B33* was redefined as 2.54×10^{-15} M, the insulin-stimulated equilibrium value of x_{12} calculated. This change was necessary to satisfy all of the constraints im-

posed by the new equilibrium after maximal insulin stimulation. Consistent with the 50% decrease in phosphotyrosine content of IRS-1 described above, this new value for PI3K is approximately one-half of that derived for the model without feedback. We chose values for V_{max}, K_d, n, and τ that seemed moderate and reasonable for introducing a time delay on the order of a few minutes. By altering these parameters, it is possible to generate behavior that ranges from biphasic changes in activity of PKC-ζ to sustained oscillations (data not shown). At present, there are no experimental data available to further refine these parameter choices.

REFERENCES

1. **Ablooglu AJ and Kohanski RA.** Activation of the insulin receptor's kinase domain changes the rate-determining step of substrate phosphorylation. *Biochemistry* 40: 504–513, 2001.

2. **Backer JM, Myers MG Jr, Shoelson SE, Chin DJ, Sun XJ, Miralpeix M, Hu P, Margolis B, Skolnik EY, Schlessinger J, and White MF.** Phosphatidylinositol 3′-kinase is activated by association with IRS-1 during insulin stimulation. *EMBO J* 11: 3469–3479, 1992.

3. **Bandyopadhyay G, Standaert ML, Sajan MP, Karnitz LM, Cong L, Quon MJ, and Farese RV.** Dependence of insulin-stimulated glucose transporter 4 translocation on 3-phosphoinositide-dependent protein kinase-1 and its target threonine-410 in the activation loop of protein kinase C-ζ. *Mol Endocrinol* 13: 1766–1772, 1999.

4. **Carpenter CL, Duckworth BC, Auger KR, Cohen B, Schaffhausen BS, and Cantley LC.** Purification and characterization of phosphoinositide 3-kinase from rat liver. *J Biol Chem* 265: 19704–19711, 1990.

5. **Charron MJ, Brosius FC III, Alper SL, and Lodish HF.** A glucose transport protein expressed predominately in insulin-responsive tissues. *Proc Natl Acad Sci USA* 86: 2535–2539, 1989.

6. **Clement S, Krause U, Desmedt F, Tanti JF, Behrends J, Pesesse X, Sasaki T, Penninger J, Doherty M, Malaisse W, Dumont JE, Le Marchand-Brustel Y, Erneux C, Hue L, and Schurmans S.** The lipid phosphatase SHIP2 controls insulin sensitivity. *Nature* 409: 92–97, 2001.

7. **Cong LN, Chen H, Li Y, Zhou L, McGibbon MA, Taylor SI, and Quon MJ.** Physiological role of Akt in insulin-stimulated translocation of GLUT4 in transfected rat adipose cells. *Mol Endocrinol* 11: 1881–1890, 1997.

8. **Cushman SW and Wardzala LJ.** Potential mechanism of insulin action on glucose transport in the isolated rat adipose cell. Apparent translocation of intracellular transport systems to the plasma membrane. *J Biol Chem* 255: 4758–4762, 1980.

9. **De Fea K and Roth RA.** Protein kinase C modulation of insulin receptor substrate-1 tyrosine phosphorylation requires serine 612. *Biochemistry* 36: 12939–12947, 1997.

10. **Ebina Y, Ellis L, Jarnagin K, Edery M, Graf L, Clauser E, Ou JH, Masiarz F, Kan YW, Goldfine ID, Roth RA, and Rutter WJ.** The human insulin receptor cDNA: the structural basis for hormone-activated transmembrane signalling. *Cell* 40: 747–758, 1985.

11. **Faure R, Baquiran G, Bergeron JJ, and Posner BI.** The dephosphorylation of insulin and epidermal growth factor receptors. Role of endosome-associated phosphotyrosine phosphatase(s). *J Biol Chem* 267: 11215–11221, 1992.

12. **Freychet P, Roth J, and Neville DM Jr.** Insulin receptors in the liver: specific binding of (^{125}I)insulin to the plasma membrane and its relation to insulin bioactivity. *Proc Natl Acad Sci USA* 68: 1833–1837, 1971.

13. **Fukumoto H, Kayano T, Buse JB, Edwards Y, Pilch PF, Bell GI, and Seino S.** Cloning and characterization of the major insulin-responsive glucose transporter expressed in human skeletal muscle and other insulin-responsive tissues. *J Biol Chem* 264: 7776–7779, 1989.

14. **Giorgetti S, Ballotti R, Kowalski-Chauvel A, Cormont M, and Van Obberghen E.** Insulin stimulates phosphatidylinositol-3-kinase activity in rat adipocytes. *Eur J Biochem* 207: 599–606, 1992.

15. **Goldstein BJ, Li PM, Ding W, Ahmad F, and Zhang WR.** Regulation of insulin action by protein tyrosine phosphatases. *Vitam Horm* 54: 67–96, 1998.

16. **Hayashi T, Okamoto M, Yoshimasa Y, Inoue G, Yamada K, Kono S, Shigemoto M, Suga J, Kuzuya H, and Nakao K.** Insulin-induced activation of phosphoinositide 3-kinase in Fao cells. *Diabetologia* 39: 515–522, 1996.

17. **Holman GD, Lo Leggio L, and Cushman SW.** Insulin-stimulated GLUT4 glucose transporter recycling. A problem in membrane protein subcellular trafficking through multiple pools. *J Biol Chem* 269: 17516–17524, 1994.

18. **Holman GD and Cushman SW.** Subcellular trafficking of GLUT4 in insulin target cells. *Seminars Cell Dev Biol* 7: 259–268, 1996.

19. **Kandel ES and Hay N.** The regulation and activities of the multifunctional serine/threonine kinase Akt/PKB. *Exp Cell Res* 253: 210–229, 1999.

20. **Karnieli E, Zarnowski MJ, Hissin PJ, Simpson IA, Salans LB, and Cushman SW.** Insulin-stimulated translocation of glucose transport systems in the isolated rat adipose cell. Time course, reversal, insulin concentration dependency, and relationship to glucose transport activity. *J Biol Chem* 256: 4772–4777, 1981.

21. **Keller SR, Kitagawa K, Aebersold R, Lienhard GE, and Garner CW.** Isolation and characterization of the 160,000-Da phosphotyrosyl protein, a putative participant in insulin signaling. *J Biol Chem* 266: 12817–12820, 1991.

22. **Kelly KL and Ruderman NB.** Insulin-stimulated phosphatidylinositol 3-kinase. Association with a 185-kDa tyrosine-phosphorylated protein (IRS-1) and localization in a low density membrane vesicle. *J Biol Chem* 268: 4391–4398, 1993.

23. **King WG, Mattaliano MD, Chan TO, Tsichlis PN, and Brugge JS.** Phosphatidylinositol 3-kinase is required for integrin-stimulated AKT and Raf-1/mitogen-activated protein kinase pathway activation. *Mol Cell Biol* 17: 4406–4418, 1997.

24. **Kublaoui B, Lee J, and Pilch PF.** Dynamics of signaling during insulin-stimulated endocytosis of its receptor in adipocytes. *J Biol Chem* 270: 59–65, 1995.

25. **Lamphere L, Carpenter CL, Sheng ZF, Kallen RG, and Lienhard GE.** Activation of PI 3-kinase in 3T3-L1 adipocytes by association with insulin receptor substrate-1. *Am J Physiol Endocrinol Metab* 266: E486–E494, 1994.

26. **Levine R.** Insulin action: 1948–80. *Diabetes Care* 4: 38–44, 1981.

27. **Levine R, Goldstein M, Klein S, and Huddlestun B.** The action of insulin on the distribution of galactose in eviscerated nephrectomized dogs. *J Biol Chem* 179: 985–990, 1949.

28. **Liu WS and Heckman CA.** The sevenfold way of PKC regulation. *Cell Signal* 10: 529–542, 1998.

29. **Madoff DH, Martensen TM, and Lane MD.** Insulin and insulin-like growth factor 1 stimulate the phosphorylation on tyrosine of a 160 kDa cytosolic protein in 3T3-L1 adipocytes. *Biochem J* 252: 7–15, 1988.

30. **Mooney RA and Anderson DL.** Phosphorylation of the insulin receptor in permeabilized adipocytes is coupled to a rapid dephosphorylation reaction. *J Biol Chem* 264: 6850–6857, 1989.

31. **Mooney RA and Green DA.** Insulin receptor dephosphorylation in permeabilized adipocytes is inhibitable by manganese and independent of receptor kinase activity. *Biochem Biophys Res Commun* 162: 1200–1206, 1989.

32. **Nystrom FH and Quon MJ.** Insulin signalling: metabolic pathways and mechanisms for specificity. *Cell Signal* 11: 563–574, 1999.

33. **Paz K, Liu YF, Shorer H, Hemi R, LeRoith D, Quon M, Kanety H, Seger R, and Zick Y.** Phosphorylation of insulin receptor substrate-1 (IRS-1) by protein kinase B positively regulates IRS-1 function. *J Biol Chem* 274: 28816–28822, 1999.

34. **Pessin JE, Thurmond DC, Elmendorf JS, Coker KJ, and Okada S.** Molecular basis of insulin-stimulated GLUT4 vesicle trafficking. Location! Location! Location! *J Biol Chem* 274: 2593–2596, 1999.

35. **Quon MJ.** Advances in kinetic analysis of insulin-stimulated GLUT-4 translocation in adipose cells. *Am J Physiol Endocrinol Metab* 266: E144–E150, 1994.

36. **Quon MJ and Campfield LA.** A mathematical model and computer simulation study of insulin receptor regulation. *J Theor Biol* 150: 59–72, 1991.

37. **Quon MJ and Campfield LA.** A mathematical model and computer simulation study of insulin-sensitive glucose transporter regulation. *J Theor Biol* 150: 93–107, 1991.

38. **Ravichandran LV, Chen H, Li Y, and Quon MJ.** Phosphorylation of PTP1B at Ser(50) by Akt impairs its ability to dephosphorylate the insulin receptor. *Mol Endocrinol* 15: 1768–1780, 2001.

39. **Ravichandran LV, Esposito DL, Chen J, and Quon MJ.** Protein kinase C-ζ phosphorylates insulin receptor substrate-1 and impairs its ability to activate phosphatidylinositol 3-kinase in response to insulin. *J Biol Chem* 276: 3543–3549, 2001.

40. **Satoh S, Nishimura H, Clark AE, Kozka IJ, Vannucci SJ, Simpson IA, Quon MJ, Cushman SW, and Holman GD.** Use of bismannose photolabel to elucidate insulin-regulated GLUT4 subcellular trafficking kinetics in rat adipose cells. Evidence that exocytosis is a critical site of hormone action. *J Biol Chem* 268: 17820–17829, 1993.

41. **Schaff J and Loew LM.** The virtual cell. *Pac Symp Biocomput*: 228–239, 1999.

42. **Scraton RE.** *Basic Numerical Methods: an Introduction to Numerical Mathematics on a Microcomputer*. London: E. Arnold, 1984.

43. **Shymko RM, De Meyts P, and Thomas R.** Logical analysis of timing-dependent receptor signalling specificity: application to the insulin receptor metabolic and mitogenic signalling pathways. *Biochem J* 326: 463–469, 1997.

44. **Shymko RM, Dumont E, De Meyts P, and Dumont JE.** Timing-dependence of insulin-receptor mitogenic versus metabolic signalling: a plausible model based on coincidence of hormone and effector binding. *Biochem J* 339: 675–683, 1999.

45. **Simpson L and Parsons R.** PTEN: life as a tumor suppressor. *Exp Cell Res* 264: 29–41, 2001.

46. **Sorisky A, Pardasani D, and Lin Y.** The 3-phosphorylated phosphoinositide response of 3T3-L1 preadipose cells exposed to insulin, insulin-like growth factor-1, or platelet-derived growth factor. *Obes Res* 4: 9–19, 1996.

47. **Stagsted J, Hansen T, Roth RA, Goldstein A, and Olsson L.** Correlation between insulin receptor occupancy and tyrosine kinase activity at low insulin concentrations and effect of major histocompatibility complex class I-derived peptide. *J Pharmacol Exp Ther* 267: 997–1001, 1993.

48. **Standaert ML, Bandyopadhyay G, Perez L, Price D, Galloway L, Poklepovic A, Sajan MP, Cenni V, Sirri A, Moscat J, Toker A, and Farese RV.** Insulin activates protein kinases C-ζ and C-λ by an autophosphorylation-dependent mechanism and stimulates their translocation to GLUT4 vesicles and other membrane fractions in rat adipocytes. *J Biol Chem* 274: 25308–25316, 1999.

49. **Standaert ML, Bandyopadhyay G, Sajan MP, Cong L, Quon MJ, and Farese RV.** Okadaic acid activates atypical protein kinase C (ζ/λ) in rat and 3T3/L1 adipocytes. An apparent requirement for activation of Glut4 translocation and glucose transport. *J Biol Chem* 274: 14074–14078, 1999.

50. **Standaert ML, Galloway L, Karnam P, Bandyopadhyay G, Moscat J, and Farese RV.** Protein kinase C-ζ as a downstream effector of phosphatidylinositol 3-kinase during insulin stimulation in rat adipocytes. Potential role in glucose transport. *J Biol Chem* 272: 30075–30082, 1997.

51. **Standaert ML and Pollet RJ.** Equilibrium model for insulin-induced receptor down-regulation. Regulation of insulin receptors in differentiated BC3H-1 myocytes. *J Biol Chem* 259: 2346–2354, 1984.

52. **Sun XJ, Miralpeix M, Myers MG Jr, Glasheen EM, Backer JM, Kahn CR, and White MF.** Expression and function of IRS-1 in insulin signal transmission. *J Biol Chem* 267: 22662–22672, 1992.

53. **Suzuki K and Kono T.** Evidence that insulin causes translocation of glucose transport activity to the plasma membrane from an intracellular storage site. *Proc Natl Acad Sci USA* 77: 2542–2545, 1980.

54. **Ullrich A, Bell JR, Chen EY, Herrera R, Petruzzelli LM, Dull TJ, Gray A, Coussens L, Liao YC, Tsubokawa M, Mason A, Seepurg PH, Grunfeld C, Rosen OM, and Ramachandran J.** Human insulin receptor and its relationship to the tyrosine kinase family of oncogenes. *Nature* 313: 756–761, 1985.

55. **Van der Kaay J, Batty IH, Cross DA, Watt PW, and Downes CP.** A novel, rapid, and highly sensitive mass assay for phosphatidylinositol 3,4,5-trisphosphate [PtdIns(3,4,5)P3] and its application to measure insulin-stimulated PtdIns(3,4,5)P3 production in rat skeletal muscle in vivo. *J Biol Chem* 272: 5477–5481, 1997.

56. **Vanhaesebroeck B and Alessi DR.** The PI3K-PDK1 connection: more than just a road to PKB. *Biochem J 346*: 561–576, 2000.

57. **Wanant S and Quon MJ.** Insulin receptor binding kinetics: modeling and simulation studies. *J Theor Biol* 205: 355–364, 2000.

58. **White MF, Shoelson SE, Keutmann H, and Kahn CR.** A cascade of tyrosine autophosphorylation in the β-subunit activates the phosphotransferase of the insulin receptor. *J Biol Chem* 263: 2969–2980, 1988.

59. **Wilden PA, Kahn CR, Siddle K, and White MF.** Insulin receptor kinase domain autophosphorylation regulates receptor enzymatic function. *J Biol Chem* 267: 16660–16668, 1992.